Global Biogeochemical Cycles

RESEARCH ARTICLE
10.1029/2021GB006961

Key Points:

- Nitrate isotope signatures in the western Arctic outflow of Polar Surface Water and eastern inflow of Atlantic Water are characterized
- Western Fram Strait is strongly stratified and nitrate deplete compared to the east where winter mixing sustains nutrient supply
- Future warming may shoal the winter mixed layer in the east, decreasing nitrate supply, and reducing primary production below current rates

Supporting Information:

Supporting Information may be found in the online version of this article.

Correspondence to:

R. E. Tuerena,
robyn.tuerena@sams.ac.uk

Citation:

Tuerena, R. E., Hopkins, J., Buchanan, P. J., Ganeshram, R. S., Norman, L., von Appen, W.-J., et al. (2021). An Arctic strait of two halves: The changing dynamics of nutrient uptake and limitation across the Fram Strait. *Global Biogeochemical Cycles*, *35*, e2021GB006961. https://doi.org/10.1029/2021GB006961

Received 26 JAN 2021
Accepted 29 JUL 2021

Author Contributions:

Conceptualization: Robyn E. Tuerena, Jo Hopkins, Pearse J. Buchanan
Data curation: Robyn E. Tuerena, Jo Hopkins, Pearse J. Buchanan, Louisa Norman, Antonia Doncila, Martin Graeve, Kai U. Ludwichowski
Formal analysis: Robyn E. Tuerena, Jo Hopkins, Pearse J. Buchanan, Louisa Norman, Antonia Doncila, Martin Graeve, Kai U. Ludwichowski

An Arctic Strait of Two Halves: The Changing Dynamics of Nutrient Uptake and Limitation Across the Fram Strait

Robyn E. Tuerena[1,2], Jo Hopkins[3], Pearse J. Buchanan[4], Raja S. Ganeshram[1], Louisa Norman[4], Wilken-Jon von Appen[5], Alessandro Tagliabue[4], Antonia Doncila[1], Martin Graeve[5], Kai U. Ludwichowski[5], Paul A. Dodd[6], Camille de la Vega[4], Ian Salter[5], and Claire Mahaffey[4]

[1]School of GeoSciences, University of Edinburgh, Edinburgh, UK, [2]Now at Scottish Association for Marine Science, Dunstaffnage, UK, [3]National Oceanography Centre, Liverpool, UK, [4]School of Environmental Sciences, University of Liverpool, Liverpool, UK, [5]Helmholtz Centre for Polar and Marine Research, Alfred Wegener Institute, Bremerhaven, Germany, [6]Norwegian Polar Institute, Framsenteret, Tromsø, Norway

Abstract The hydrography of the Arctic Seas is being altered by ongoing climate change, with knock-on effects to nutrient dynamics and primary production. As the major pathway of exchange between the Arctic and the Atlantic, the Fram Strait hosts two distinct water masses in the upper water column, northward flowing warm and saline Atlantic Waters in the east, and southward flowing cold and fresh Polar Surface Water in the west. Here, we assess how physical processes control nutrient dynamics in the Fram Strait using nitrogen isotope data collected during 2016 and 2018. In Atlantic Waters, a weakly stratified water column and a shallow nitracline reduce nitrogen limitation. To the west, in Polar Surface Water, nitrogen limitation is greater because stronger stratification inhibits nutrient resupply from deeper water and lateral nitrate supply from central Arctic waters is low. A historical hindcast simulation of ocean biogeochemistry from 1970 to 2019 corroborates these findings and highlights a strong link between nitrate supply to Atlantic Waters and the depth of winter mixing, which shoaled during the simulation in response to a local reduction in sea-ice formation. Overall, we find that while the eastern Fram Strait currently experiences seasonal nutrient replenishment and high primary production, the loss of winter sea ice and continued atmospheric warming has the potential to inhibit deep winter mixing and limit primary production in the future.

Plain Language Summary The Fram Strait is the main gateway of the Arctic Ocean. In the east, warm, salty waters from the Atlantic flow north into the Arctic basin, and in the west, cold, fresh waters flow south from the central Arctic into the North Atlantic. We examined how changes to the availability of nutrients (which are essential for algae to grow) may limit algae growth in the Fram Strait, both as a result of changes to their source and also how easily the upper ocean mixes nutrients from depth. In the eastern Fram Strait, there is a high availability of nitrate, one of the main nutrients to support algae growth, and winter mixing sustains nutrient supply and biological production in recent decades. However, in the western Fram Strait, the outflowing surface waters do not easily mix with deeper waters and are depleted in nitrate, and nutrient supply from the central Arctic has been declining in recent decades. Our work suggests that although the eastern Fram Strait is sustaining higher levels of algae growth, which supports fisheries and higher trophic levels, warming over the coming decades could shoal winter mixed layers enough to decrease summertime nutrients and limit biological production.

1. Introduction

Arctic primary production has increased by >50% in the last two decades, fueled by increased light and nutrient availability, but whether or not this trend continues will depend on a sustained nutrient supply to phytoplankton (Arrigo & van Dijken, 2015; Lewis et al., 2020). Currently, nitrogen (N) is the main limiting nutrient to phytoplankton in the Arctic Ocean (Krisch et al., 2020; Mills et al., 2018). As warming continues, the degree of N limitation may change as the water mass properties supplied from the Atlantic and Pacific are altered (Hatún et al., 2017; Woodgate, 2018). Stable isotope measurements of nitrate and organic nitrogen can be used to provide insights into past and present N limitation to phytoplankton (Francois

Funding acquisition: Jo Hopkins, Raja S. Ganeshram, Alessandro Tagliabue, Claire Mahaffey
Project Administration: Claire Mahaffey
Writing – original draft: Robyn E. Tuerena, Jo Hopkins, Pearse J. Buchanan
Writing – review & editing: Robyn E. Tuerena, Jo Hopkins, Pearse J. Buchanan, Raja S. Ganeshram, Wilken-Jon von Appen, Alessandro Tagliabue, Paul A. Dodd, Camille de la Vega, Ian Salter, Claire Mahaffey

et al., 1997; Tuerena et al., 2021). Here, we use these tools to decipher how nutrient limitation is changing in the Fram Strait.

The Fram Strait is both an inflow and outflow gateway to the Arctic Ocean. In the east, warm and saline Atlantic Water (AW) that originates from the subpolar and subtropical North Atlantic gyres is transported northward within the West Spitsbergen Current (WSC) and enters the Arctic Ocean north of Svalbard. The WSC is a complex, eddy-shedding (von Appen et al., 2016), multibranch system with both barotropic and baroclinic components (Beszczynska-Möller et al., 2012; Richter et al., 2018) that keeps the eastern Fram Strait ice free for most of the year. In the upper layers of the WSC, the AW has been observed to be warming since the mid-1990s at a rate of 0.06°C year^{-1} and also increasing in salinity (Beszczynska-Möller et al., 2012; Larsen et al., 2016; Polyakov et al., 2017; Tsubouchi et al., 2021; Walczowski et al., 2017). Warming of AW has been driven by a combination of both a local response to increasing air temperatures and reduced heat loss (Furevik, 2001; Karcher et al., 2005), and a greater proportion of subtropical water being transported into the Nordic Seas (Hatún et al., 2005). Carried by the boundary current in the Eurasian Basin, this warming signal is progressing into the Arctic Ocean and increasing heat fluxes to overlying water, which weakens the halocline, increases winter ventilation of the ocean interior, and accelerates sea-ice decline (Polyakov et al., 2017, 2020; Steele & Boyd, 1998). These changes drive an increase in nutrient supply, supporting the view that areas experiencing "Atlantification" may become more productive (Ardyna et al., 2014; Randelhoff et al., 2015, 2018, 2020). However, further warming, notably in regions that have already become ice free, could lead to increased stratification and decreased nutrient supply, ultimately controlling nutrient availability to Arctic phytoplankton with subsequent influence on productivity.

On the western side of the Fram Strait, the East Greenland Current (EGC) system (Havik et al., 2017) transports cold, fresh Arctic origin water and sea ice southward into the subpolar North Atlantic Ocean. The Polar Surface Water (PSW) in the upper 200 m of the EGC consists of riverine input, sea-ice melt, and Pacific origin water (Dodd et al., 2012; Haine et al., 2015). The shelf break and offshore branches of the EGC also transport deeper Arctic Atlantic Water (AAW), an Atlantic derived water mass that has entered the Arctic Ocean and been modified during transit within the boundary current and passage across Arctic shelves (Wefing et al., 2019). Local westward recirculation of AW within Fram Strait (RAW; recirculated Atlantic Water), mediated by high eddy activity, joins the AAW and significantly increases the southward transport of the shelf break branch of the EGC (de Steur et al., 2014; Havik et al., 2017; Richter et al., 2018). Modeling studies reveal interannual to decadal scale variability in freshwater export from the Fram Strait. However, improvements to the simulation of salinity anomalies are needed in order to make robust estimates of long-term trends (Jahn et al., 2012; Karcher et al., 2005). Observations suggest that the freshwater flux within the EGC was relatively stable between 1998 and 2008, but transport over the wide East Greenland Shelf where the freshest waters are found was not accounted for (de Steur et al., 2009). The salinity of polar water over the East Greenland Shelf may have been decreasing since the mid-2000s (Larsen et al., 2016). At the surface, the EGC transports relatively high silicate and phosphate, but low nitrate, a signature that is due to Pacific-water influence and amplified by benthic denitrification on Arctic shelves (Chang & Devol, 2009; Devol et al., 1997). The depleted nitrate concentrations in PSW are the main limiter to net primary production (NPP) in this region (Krisch et al., 2020). Higher nitrate concentrations are found in Atlantic origin water that intrudes across the shelf along the bottom (Hattermann et al., 2016). Any increases in freshwater input and/or surface warming that strengthen stratification across the western side of Fram Strait may suppress vertical mixing and limit the supply of bottom water nitrate to the surface.

These east-west differences across Fram Strait produce gradients in the physical and biogeochemical processes which control NPP. In the now ice-free eastern Fram Strait, annual NPP is ~80 g C m^{-2} (Hop et al., 2006) compared to 50–100 g C m^{-2} in partially ice-covered waters in the middle of the strait (Wassmann et al., 2010) and ~15 g C m^{-2} (Codispoti et al., 2013) in the ice-covered PSW in the western Fram Strait. As the freshwater, heat and volume transports both into and out of the Arctic Ocean via the Fram Strait continue to be altered and the biogeochemical composition of these waters changes, there is a need to understand the impact on nutrient supply and the implications for NPP, both now and in the future. Nitrogen isotope measurements provide a tool to help address this challenge.

Nitrate isotope measurements estimate the relative contributions of NPP, remineralization, and denitrification to the nitrate present in the water column. The $^{15/14}$N and $^{18/16}$O in nitrate (δ^{15}N-NO_3 and δ^{18}O-NO_3,

respectively) provide complementary information about nitrate uptake and regeneration processes (Rafter et al., 2013; Sigman, DiFiore, Hain, Deutsch, & Karl, 2009). Fractionation of nitrogen and oxygen atoms occurs at the same rate (ε) during uptake of nitrate by phytoplankton (~5‰) (Tuerena et al., 2015; Waser et al., 1998) and during denitrification (25‰–30‰) (Sigman, DiFiore, Hain, Deutsch, Wang, et al., 2009). When nitrate is newly nitrified (i.e., produced from recently remineralized organic matter), the nitrogen atoms are unchanged and reflect the isotopic signature of organic matter, which varies in response to local conditions. In contrast, oxygen atoms are sourced from the oxidation of ambient O_2 and seawater, providing a predictable nitrification signature of $\delta^{18}O\text{-}H_2O$ plus 1.1‰ (Buchwald et al., 2012; Sigman, DiFiore, Hain, Deutsch, & Karl, 2009). Isotopic signatures of nitrogen and oxygen in nitrate therefore diverge in waters with strong recycling, with a relative decrease in $\delta^{18}O\text{-}NO_3$. The tracer $\Delta(15\text{–}18)$ ($\delta^{15}N\text{-}NO_3$ minus $\delta^{18}O\text{-}NO_3$) captures the differences between these two isotopes, highlighting nitrate sources from different oceanic environments (Rafter et al., 2013). A specific process in the Arctic affecting $\Delta(15\text{–}18)$ is benthic denitrification, which can release high $\delta^{15}N\text{-}NH_4$ into the water column, a process termed coupled partial nitrification–denitrification (Brown et al., 2015; Fripiat et al., 2018; Granger et al., 2018). This process leads to an increase in $\delta^{15}N\text{-}NO_3$, a decrease in $\delta^{18}O\text{-}NO_3$ (via water column nitrification), and a concomitant increase in $\Delta(15\text{–}18)$.

The uptake of nitrate by phytoplankton can often be described by Rayleigh fractionation systematics (Mariotti et al., 1981). Nitrate utilization by phytoplankton in an environment where there is no resupply of nutrients, that is, a stratified upper ocean in summer, follows Rayleigh fractionation systematics for a closed system, with $\delta^{15}N\text{-}NO_3$ and $\delta^{18}O\text{-}NO_3$ increasing in a 1:1 relationship as nitrate is consumed. The slope of this line is dependent on the isotopic effect (ε) (Granger et al., 2004). As nitrogen is consumed to completion, the N isotopic signature in organic matter ($\delta^{15}N\text{-}PN$) will approach that of the inorganic nitrogen at the beginning of the growing season plus the isotopic effect, which for phytoplankton assimilation is 5‰. When the upper ocean is less stratified, $\delta^{15}N\text{-}NO_3$ and $\delta^{18}O\text{-}NO_3$ can represent open system dynamics where there is continual resupply of nutrients through the growing season. In this situation, the isotopic enrichment of $\delta^{15}N\text{-}PN$ is weaker as new nitrogen with a lower isotopic signature is continually supplied. Applying closed system assumptions to an open system will result in an apparent isotope effect weaker than 5‰. Thus, in combination with nitrate isotopes, $\delta^{15}N\text{-}PN$ can track the extent of biological utilization, contrasting nutrient sources, and the significance of new versus regenerated production.

This study characterizes the nitrogen cycling processes occurring in the upper waters of Fram Strait in spring and summer. We focus on the AW and PSW entering and exiting the Arctic, respectively. We utilize a combination of biogeochemical tracers, $\delta^{15}N\text{-}NO_3$, $\delta^{18}O\text{-}NO_3$, $\Delta(15\text{–}18)$, $\delta^{15}N\text{-}PN$, N* (N* = nitrate-phosphate•16 Gruber & Sarmiento, 1997) and Si* (Si* = silicate-nitrate Sarmiento et al., 2004), alongside hydrographic data (temperature, salinity, and mixed layer depth [MLD]) from two cruises in spring and summer to explore nitrogen availability to phytoplankton and the implications for primary production. Different nutrient supply mechanisms in the region are more broadly characterized using results from a historical hindcast simulation with a global ocean biogeochemical model from 1970 to 2019. We draw upon the simulations to discuss the implications of warming to Arctic nutrient availability and primary production in the future.

2. Materials and Methods

2.1. Fieldwork

This work is based on samples collected on two cruises in the Fram Strait region. Cruise PS100 took place from June 18 to September 6, 2016, and JR17005 took place between May 8 and June 8, 2018 (Figure 1a). Cruise PS100 was conducted on the R/V Polarstern as part of the larger GEOTRACES program (Schlitzer et al., 2018). Cruise JR17005 took place on the *RRS* James Clark Ross as part of the UK Changing Arctic Oceans program. Although the two seasons sampled were not in the same year, they were both in years of relatively small April sea-ice area export through the Fram Strait (Mayot et al., 2020). Although we treat these cruises as representative of late spring and late summer, we acknowledge that this is an assumption and cannot account for interannual variability in the onset of seasonal changes. On both cruises, seawater samples were collected from Niskin bottles mounted on a rosette equipped with a SBE911plus CTD system recording conductivity, temperature, and pressure at 24 Hz (Hopkins et al., 2019; Kanzow et al., 2017).

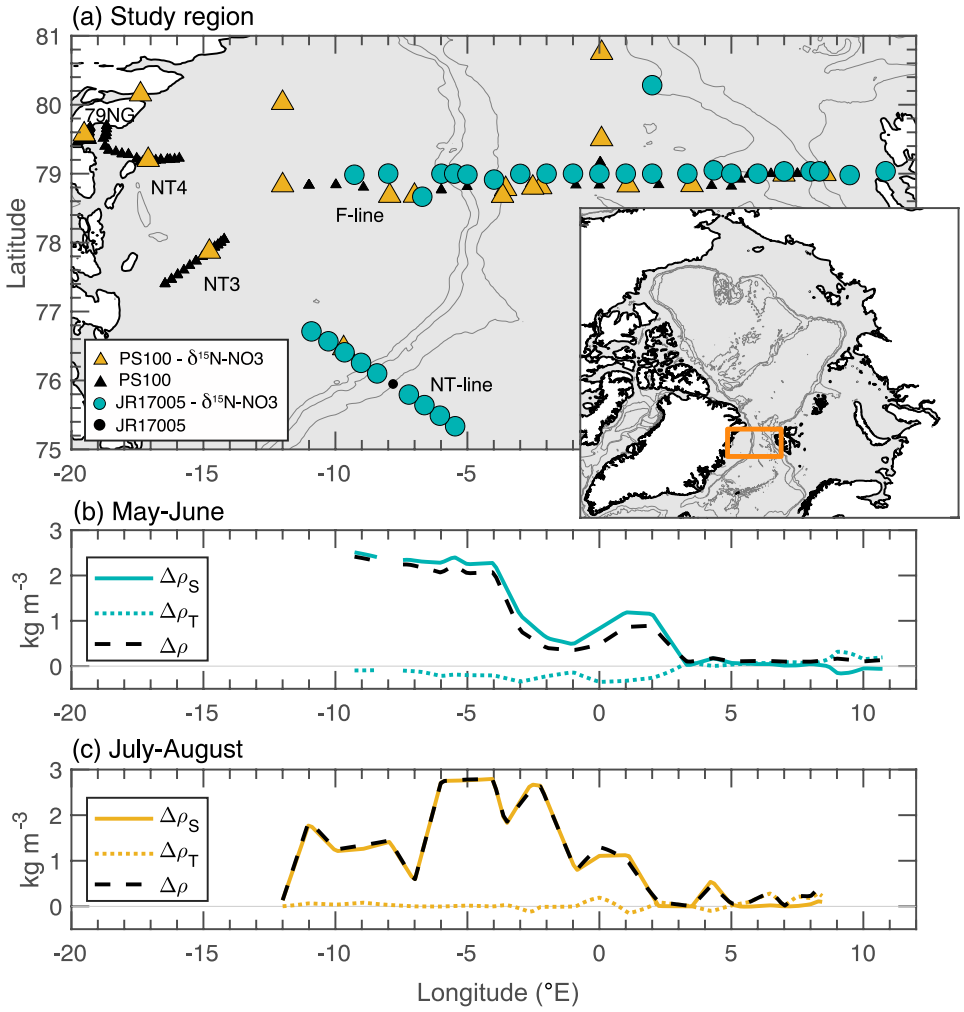

Figure 1. (a) Map of study region. Samples from cruise JR17005 are highlighted in cyan and were collected between May and June 2018 onboard the RRS James Clark Ross. Samples from cruise PS100 are highlighted in orange and were collected in July–August 2016 onboard the RV Polarstern. Extra stations from these cruises are shown with smaller black triangles and dots. The boxes highlight the sections used in Figures 2 and 3. (b, c) Strength of stratification across the Fram Strait expressed as the potential density difference between 10 and 200 m depth in (b) May–June 2018 (JR17005) and (c) July–August 2016 (PS100). Thermal ($\Delta\rho_T$; dashed) and haline ($\Delta\rho_S$; solid) contributions to the potential density difference ($\Delta\rho_S$; dashed black) are shown for each season.

Salinity was calibrated onboard with discrete samples using an Autosal 8400B salinometer (Guildline) on JR17005 and an Optimare Precision Salinometer (Optimare) on PS100.

Both cruises completed a transect across the Fram Strait at ~79°N (F-Line, Figure 1a). On JR17005, a cross-shelf transect running up the Norske Trough (NT Line) was also sampled. On PS100 sampling across the Norske Trough, further on-shelf (NT3 and NT4) was possible and a section along the front of the 79°N glacier (79NG) was completed. The extra sections are included in Figures S1 and S2 and are included in our statistical comparisons of AW and PSW (Table 1).

We quantified the stability of the upper water column to vertical displacements according to the Brunt-Väisälä frequency, N^2:

$$N^2 = -\frac{g}{\rho}\frac{\partial \rho}{\partial z} \quad (1)$$

where g is the gravitational acceleration, ρ is the potential density, and z is the depth. N^2 was estimated at a 1-m resolution, with higher values indicating stronger stratification. Strength of stratification was also

Table 1
Water Mass Classifications and Average Values, as Defined in Richter et al. (2018)

Water mass	Definition	Nitrate (μM)	N* (μM)	Si* (μM)	δ^{15}N-NO_3 (‰)	δ^{18}O-NO_3 (‰)	Δ(15–18) (‰)	δ^{15}N-PN (‰)
AW	Depth > 150 m	11.6 ± 0.8	−1.4 ± 1.4	−7.1 ± 0.7	5.1 ± 0.2	2.4 ± 0.3	2.7 ± 0.4	
$\theta > 2$, $27.7 < \sigma_\theta \leq 27.97$	Spring, mixed layer	5.1 ± 4.0	−2.4 ± 1.3	−2.7 ± 3.3				3 ± 1.2
$\sigma_\theta < 27.7$, $S > 34.92$	Summer, mixed layer	0.9 ± 1.3	−1.7 ± 0.4	−0.1 ± 0.7				3.1 ± 2.5 (July–Aug)3.6 ± 0.5 (Aug–Sep)
PSW	Depth > 75 m	7.2 ± 2.3	−4.4 ± 2.4	−1.4 ± 2.7	5.5 ± 0.4	1.3 ± 0.4	4.2 ± 0.7	
$\theta < 0$, $\sigma_\theta < 27.7$	Spring, mixed layer	1.6 ± 1.3	−4.7 ± 2.7	1.7 ± 2.6				4.5 ± 0.9
	Summer, mixed layer	0.5 ± 0.4	−6 ± 1.3	4.5 ± 2.1				5.3 ± 1 (July–Aug)5.4 ± 0.3 (Aug–Sep)

Note. AW, Atlantic Water; PSW, Polar Surface Water. Boundaries of potential temperature (θ) are in °C and potential density (σ_θ) are in kg m^{-3}. This definition also captures AW that has recirculated locally within the Fram Strait and has been entrained within the EGC system. No values are added to δ^{15}N-NO_3, δ^{18}O-NO_3, and Δ(15–18) during spring and summer, as their water mass characteristics are best described below the mixed layer and away from the effects of spring/summer uptake; δ^{15}N-PN values are not shown for below the mixed layer as these values would be influenced by regeneration. Samples collected from two cruises in summer 2016 were used to estimate δ^{15}N-PN to increase the confidence of our statistics, those from July to August were collected from cruise PS100 and those from August to September were collected from cruise NPI-16. All other values in summer are from cruise PS100.

assessed by calculating the difference in potential density between 10 and 200 m depth, $\Delta\rho$ (Figures 1b and 1c). The thermal ($\Delta\rho_T$) and haline ($\Delta\rho_S$) contributions to this density difference, where $\Delta\rho \sim \Delta\rho_T + \Delta\rho_S$, were estimated as follows:

$$\Delta\rho_T = -\alpha\rho\left(T_2 - T_1\right) \quad (2)$$

$$\Delta\rho_S = \beta\rho\left(S_2 - S_1\right) \quad (3)$$

where α and β are the thermal expansion and haline contraction coefficients, respectively, calculated at the average temperature, salinity, and pressure between 10 and 200 m. Subscripts 1 and 2 refer respectively to surface (10 m) and 200 m depth values of temperature (T) and salinity (S) and ρ is the average potential density between 10 and 200 m. The surface MLD was calculated following Peralta-Ferriz and Woodgate (2015), defined as the maximum depth at which the potential density was within 0.01 kg m^{-3} of the shallowest measurement. On both cruises, the shallowest measurement was always within 5 m of the surface. The MLD did not exceed 200 m on either cruise.

Dissolved inorganic nutrient concentrations from JR17005 were determined using a Bran and Luebbe QuAAtro 5-channel autoanalyser (SEAL Analytical) and AACE operating platform (V 6.1) following standard colorimetric methods. Nutrient concentrations from PS100 are publicly available in the Pangaea database (Graeve & Ludwichowski, 2017). Nitrate isotope samples were filtered inline from the Niskin bottles (0.7 μm pore size filters) and frozen at −20°C until analysis on land. Nitrate samples were measured for δ^{15}N-NO_3 and δ^{18}O-NO_3 using the denitrifier method and bacterial strain *Pseudomonas aureofaciens* (Casciotti et al., 2002; Sigman et al., 2001). Samples were corrected using international reference standards IAEA-N3 and USGS-34 and an internal standard of North Atlantic Deep Water was run with each batch to check for interrun comparability. Final values for both cruises were calculated using the correction scheme of Weigand et al. (2016) with reproducibility of 0.1‰ and 0.3‰ for δ^{15}N-NO_3 and δ^{18}O, respectively. Nitrite concentrations in our study region ranged from 0 to 0.32 μM and 91% of nitrate isotope samples had a <2% contribution of nitrite to the nitrate + nitrite pool (215/235 samples). Our isotopic measurements are compared to studies in which the nitrite in a sample has been removed using sulfamic acid (Granger & Sigman, 2009); to account for this, we correct our δ^{18}O-NO_3 data for nitrite interference following Kemeny et al. (2016). The δ^{15}N-NO_3 + NO_2 samples were also corrected assuming a δ^{15}N-NO_2 of −24‰ (Kemeny et al., 2016; Tuerena et al., 2021). All samples with a high contribution (>2%) of nitrite were in the upper 50 m and were therefore not used for water mass averages.

δ^{15}N-PN from JR17005 was determined by EA-IRMS using a Costech Instruments Elemental Analyzer coupled to Thermo Scientific Delta V Advantage mass spectrometer fitted with Conflo IV gas handling system. The instrumentation was operated using ISODAT 3.0 isotope ratio MS software. Prior to analysis, the filters were wrapped in tin foil cones (OEA Laboratories) and pelletized. δ^{15}N-PN from PS100 were analyzed with elemental analyzer (Thermo Flash 2000) coupled to an isotope ratio mass spectrometer (Thermo, Delta V Plus). Additional δ^{15}N-PN samples were collected from the Norwegian Polar Institute cruise of Fram Strait in August–September 2016 and analyzed using a Carlo Erba NA 2500 elemental analyzer inline with a VG PRISM III isotope ratio mass spectrometer. The inclusion of these additional summer samples provides 125% more summer measurements and increases confidence in statistics (see Table 1).

Within regions on the eastern (3°–8°E) and western (6°–10°W) sides of the Fram Strait that were sampled on both cruises, we calculate the depth of the top and bottom of the nitracline following Randelhoff et al. (2016). First, the nitrate samples were interpolated onto a 1-m-resolution vertical grid. The top and bottom of the nitracline were then defined as the depth where the nitrate concentration was 20% and 80%, respectively, of the difference between surface and deep reference values. The surface reference value was taken as the average concentration over the top 15 m of the water column. The deep reference value was taken as the average concentration between 90 and 160 m on the eastern side of the Fram Strait and between 140 and 200 m depth on the western side of Fram Strait, a depth range occupied by Atlantic origin water. With the exception of the eastern side of the Fram Strait in May–June, these deep references were below the base of the mixed layer and the depth of maximum N^2. In May–June, although the mixed layer over the deep basin on the eastern side of the Fram Strait was often greater than 160 m, nitrate within the 90–160 m reference interval was homogeneously distributed and the average concentrations were above 10 μM.

To quantify the different nutrient concentrations, nutrient ratios, and isotopic values of AW and PSW, we defined the water mass type of each sample using the water mass properties defined in Richter et al. (2018) and summarized in Table 1. We explicitly exclude samples collected within AAW whose signatures may have been modified within the Arctic basin. Note also that the definition of AW used here (see Table 1) includes Atlantic origin water that has recirculated locally within the Fram Strait (RAW) and has been entrained within the EGC system.

2.2. Hindcast Simulation

We used the Pelagic Interactions Scheme for Carbon and Ecosystem Studies version 2 (PISCES-v2) biogeochemical model (Aumont et al., 2015), attached to the Nucleus for European Modeling of the Ocean version 4.0 (NEMO-v4) general ocean circulation model and the Sea Ice modeling Integrated Initiative (SI^3) sea-ice model. The biogeochemical model carries two phytoplankton types (nanophytoplankton and diatoms), two zooplankton types (microzooplankton and mesozooplankton), large and small particulate organic matter, dissolved organic matter, oxygen, carbon chemistry tracers, and five nutrients (nitrate, ammonium, silicate, phosphate, and iron). The nitrogen cycle accounted for nitrogen fixation, atmospheric deposition, river inputs, nitrification, sedimentary and water column denitrification, and burial. Nitrogen isotopes were integrated within PISCESv2 to enable direct comparison with field data (Text S1). Latitudinal resolution on the tripolar grid was nominally 2° but increased to 0.5° at the equator and 1° poleward of 50° (in Fram Strait the resolution was ∼5° longitude by 0.9° latitude [∼100 km^2] which is not eddy-resolving), while vertical resolution varied between 10 and 500 m thickness over 31 levels. We forced the coupled NEMO–SI^3–PISCES model with the Japanese atmospheric reanalysis (JRA-55) over the years 1958–2019 (Tsujino et al., 2018) following the Ocean Modeling Intercomparison Project protocols (Orr et al., 2017). Six repeat cycles of this 62-year forcing (372 years) were made beginning on the January 1, 1648 CE, ending on December 31, 2019, with the ocean biogeochemical initial state taken from a 5,000 years spin-up simulation under preindustrial conditions. Only output in the final cycle was used in analysis, and because the final cycle was initialized with the end of the fifth cycle, we only included the period 1970–2019 in our analysis to avoid unrealistic trends due to adjustment at the beginning of the final cycle.

While the resolution of the model did not resolve the observed eddy kinetic energy field, the baroclinic component of the boundary currents or fine-scale AW recirculation pathways (Beszczynska-Möller et al., 2012; Richter et al., 2018; von Appen et al., 2016), it did simulate realistic trends in temperature and salinity in the west and east of the northern Greenland Sea. However, due to a weak WSC, the east Fram Strait at 79°N

was dominated by PSW rather than AW. To overcome this local inconsistency, we assessed hydrographic and biogeochemical properties within the AW and PSW water masses over the Greenland Sea between 22°W–15°E and 70°N–80°N. AW was defined as warmer than 2°C and saltier than 34.5 psu, while PSW was defined as cooler than 0°C and fresher than 33.5 psu. These property bounds are slightly different to those in the field data (Table 1) but were chosen to best represent these water masses in the model (Figure S3). Temperature and salinity trends within each water mass were assessed in the mixed layer, defined by the 0.01 kg m^{-3} density change. We assume that the depth of the mixed layer in winter is a reasonable proxy for the maximum depth of winter mixing. Simulated nitrate concentrations and its isotopes were assessed in the upper 50 m because summer euphotic and MLDs were consistently shallower than 50 m and 98% of all NPP occurred within the upper 50 m. This water mass approach, rather than a transect approach, enabled a more direct comparison between simulated and observed AW and PSW.

3. Results

3.1. Water Mass Characterization, Mixed Layer Depths, and Stratification

The strength of stratification across the Fram Strait within the upper 200 m of the water column increased from east to west in both seasons (Figures 1b and 1c). On the eastern side of the strait, relatively weak upper ocean stratification in Atlantic origin water was maintained by the thermal contribution to vertical density differences. This thermal control leads to deep convection during the cold winter months and thermal stratification in the summer. To the west of the AW-PSW front, the fresher Arctic sourced surface waters resulted in a much more strongly stratified water column. Note that during May–June, the vertical temperature gradient on the western side of the Strait was unstable (i.e., it made a negative contribution to stability).

Figures 2a, 2b, 3a and 3b show the potential temperature and salinity across the Fram Strait and East Greenland Shelf from the May–June 2018 to July–August 2016 cruises, respectively. The eastern side of Fram Strait was dominated by warm (>2°C) AW. The core of the AW is carried northward within the WSC concentrated over the 450–500 m isobath (8°E). The surface layer on the west of Fram Strait and over the East Greenland Shelf was dominated by PSW. The PSW layer was deepest over the shelf (200 m) and gradually shoaled to 50 m depth as it extended eastward beyond the shelf edge. The transition between surface AW to the east, that had never interacted with sea ice, and outflowing PSW in May–June 2018 took place around 3°E. During July–August 2016, this frontal boundary occurred further west at 1°W and meltwater extended to 2°E. The AAW was found below AW/RAW (between 250 and 500 m) on the upper slope of the Greenland continental shelf and across the shelf below the PSW layer in July–August 2016.

Spring to summer changes in MLD, the depth of maximum N^2, and the depth of the top and bottom of the nitracline on the eastern and western sides of Fram Strait are summarized in Figure 4. Early in the season between May and June, the MLD on the eastern side of the Strait ranged between 120 and 180 m, with some shallower and deeper instances (Figures 2a and 4e). Although surface warming had started to establish a weak peak in N^2 at around 30 m (Figure 4e), the surface temperature was <4°C (Figure 2a), and the resulting vertical density differences associated with this near surface warming were not sufficient to be identified as the MLD according to the threshold used here. The nitracline was found between 40 m (top) and 70 m (bottom), just below the maximum in N^2, but above the MLD (Figure 4e). The surface chlorophyll-*a* fluorescence signal in spring was well mixed down to the top of the nitracline (maximum in N^2) and then gradually decreased toward the base of the nitracline (Figure 4d). In the summer, surface water temperatures increased above 6°C (Figure 3a) and stratification strengthened (Figures 4a and 4b), leading to a much more clearly defined mixed layer at ∼20 m, coincident with the maximum in N^2 (Figure 4e). Both the top and bottom of the nitracline also shoaled by ∼10 m but remained below the MLD. A subsurface chlorophyll-*a* fluorescence maximum was observed at the base of the surface mixed layer (Figure 4d).

In contrast to the large seasonal change in MLD observed on the eastern side of Fram Strait, the spring to summer change in MLD on the western side of Fram Strait (in PSW) was smaller. In spring, a 20–40 m well-mixed surface layer overlaid a broad (60–70-m-thick) pycnocline, which typically extended below the top of the nitracline (Figure 4j). During the summer, warming of a thin PSW layer (potential temperature >0°C) and the addition of sea-ice melt established a MLD and maximum value of N^2 between 10 and 20 m (Figure 4j). This shallow surface layer was decoupled from the nitracline below (30–110 m). There was little

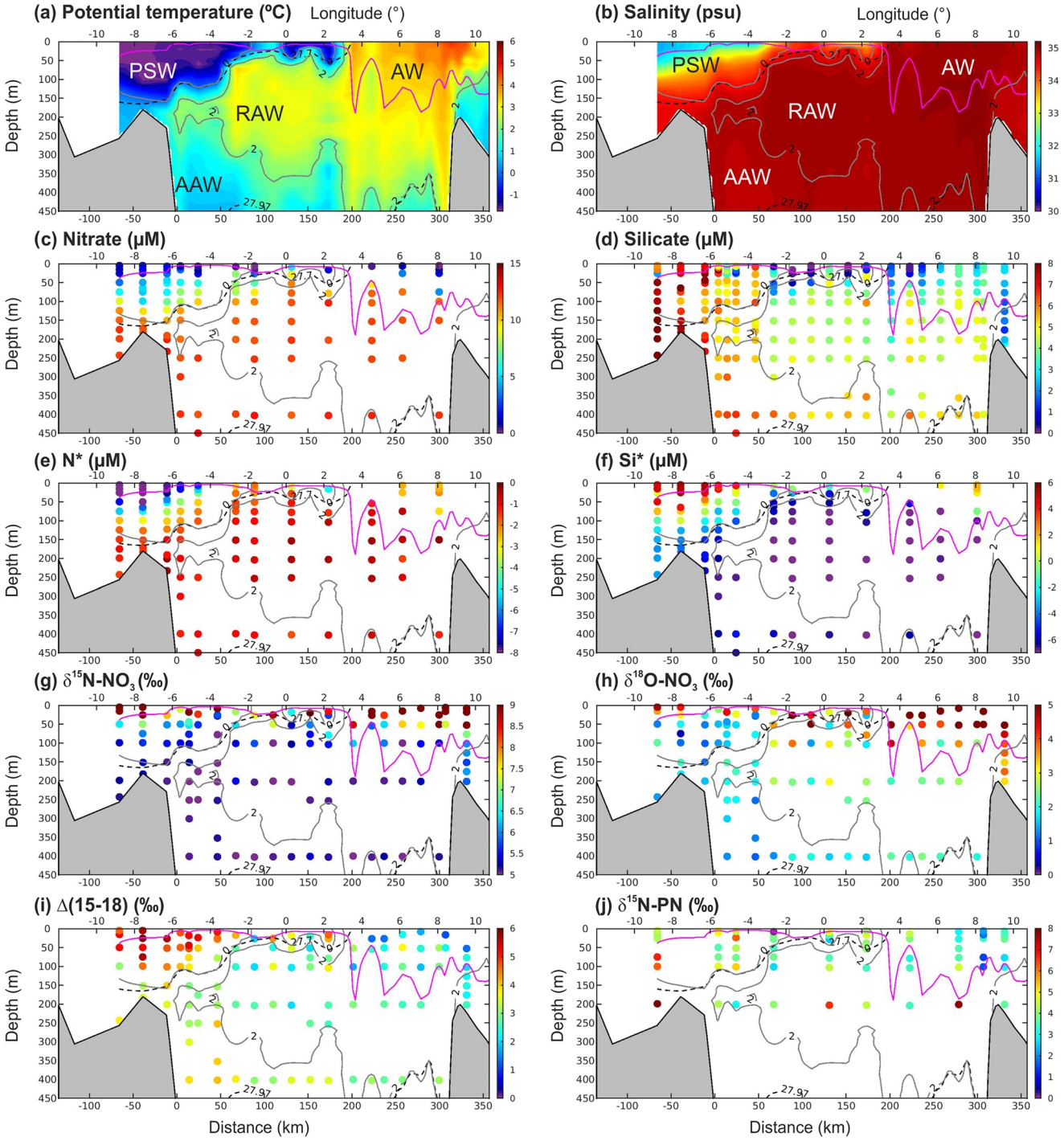

Figure 2. Sections of the upper 450 m across the Fram Strait (F-Line) from cruise JR17005 during May–June 2018. (a) Temperature, (b) Salinity, (c) Nitrate (μM), (d) Silicate (μM), (e) N* (μM), (f) Si* (μM), (g) δ^{15}N-NO_3 (‰ vs. AIR), (h) δ^{18}O-NO_3 (‰ vs. VSMOW), (i) Δ(15–18) (‰), and (j) δ^{15}N-PN (‰ vs. AIR). The mixed layer depth is shown with a magenta line in each plot. Key isotherms (gray contours) and isopycnals (dashed black contours) used to define water masses are overlaid. Atlantic Water (AW), Polar Surface Water (PSW), Arctic Atlantic Water (AAW), and recirculated Atlantic Water (RAW) are marked.

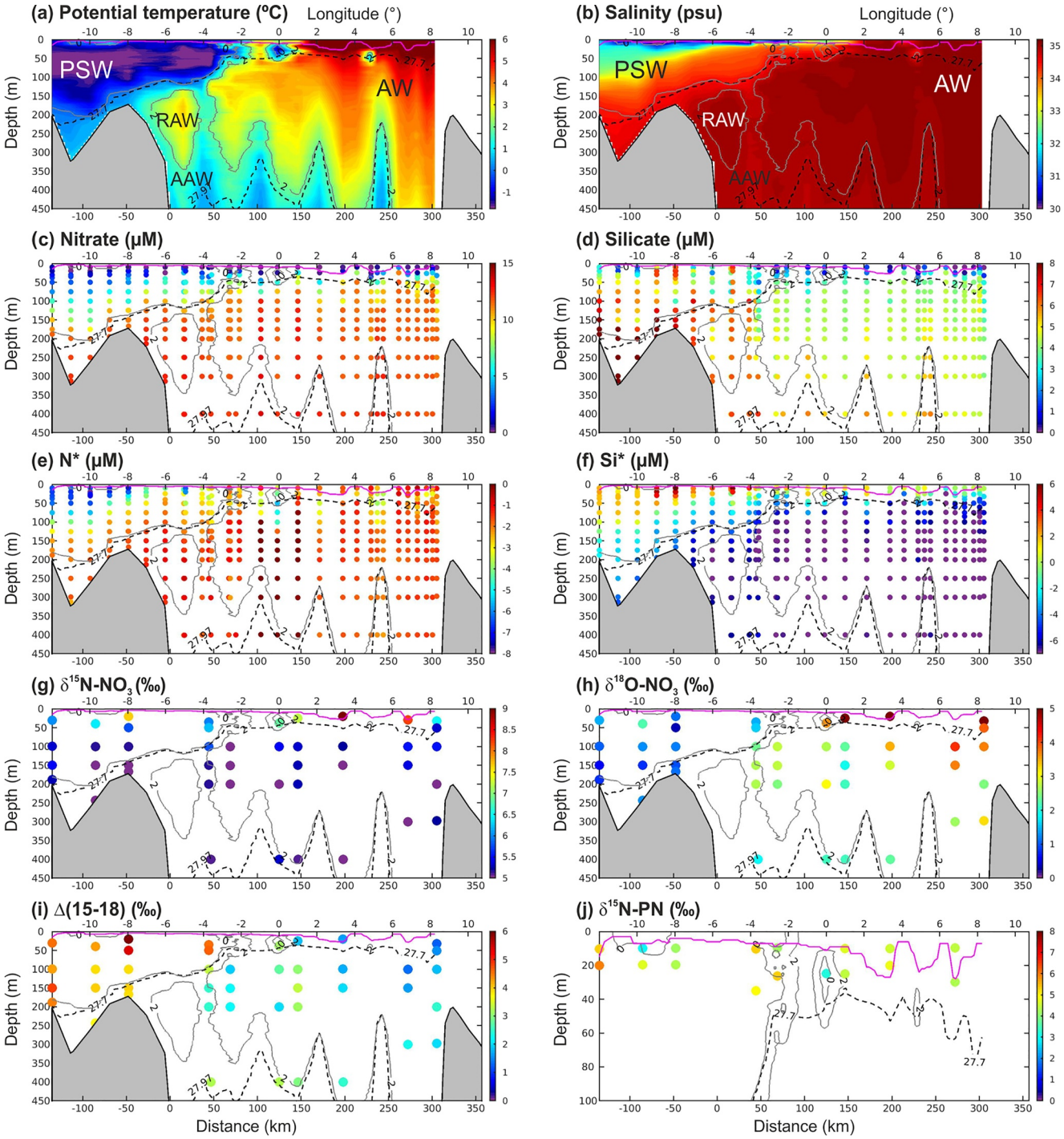

Figure 3. Sections of the upper 450 m across the Fram Strait from cruise PS100 during July–August 2016. (a) Temperature, (b) Salinity, (c) Nitrate (μM), (d) Silicate (μM), (e) N* (μM), (f) Si* (μM), (g) δ^{15}N-NO_3 (‰ vs. AIR), (h) δ^{18}O-NO_3 (‰ vs. VSMOW), (i) Δ(15–18) (‰), and (j) δ^{15}N-PN (‰ vs. AIR). Contours and labeling as per Figure 2.

change in the depth of the top and bottom of the nitracline between spring and summer. The surface chlorophyll-*a* fluorescence signal in spring was well mixed throughout the surface mixed layer and gradually decreased within the broad pycnocline. During the summer, two subsurface peaks in chlorophyll-*a* fluorescence were observed: the shallowest just below the surface mixed layer and N^2 maximum and a second, deeper and weaker peak within the nitracline.

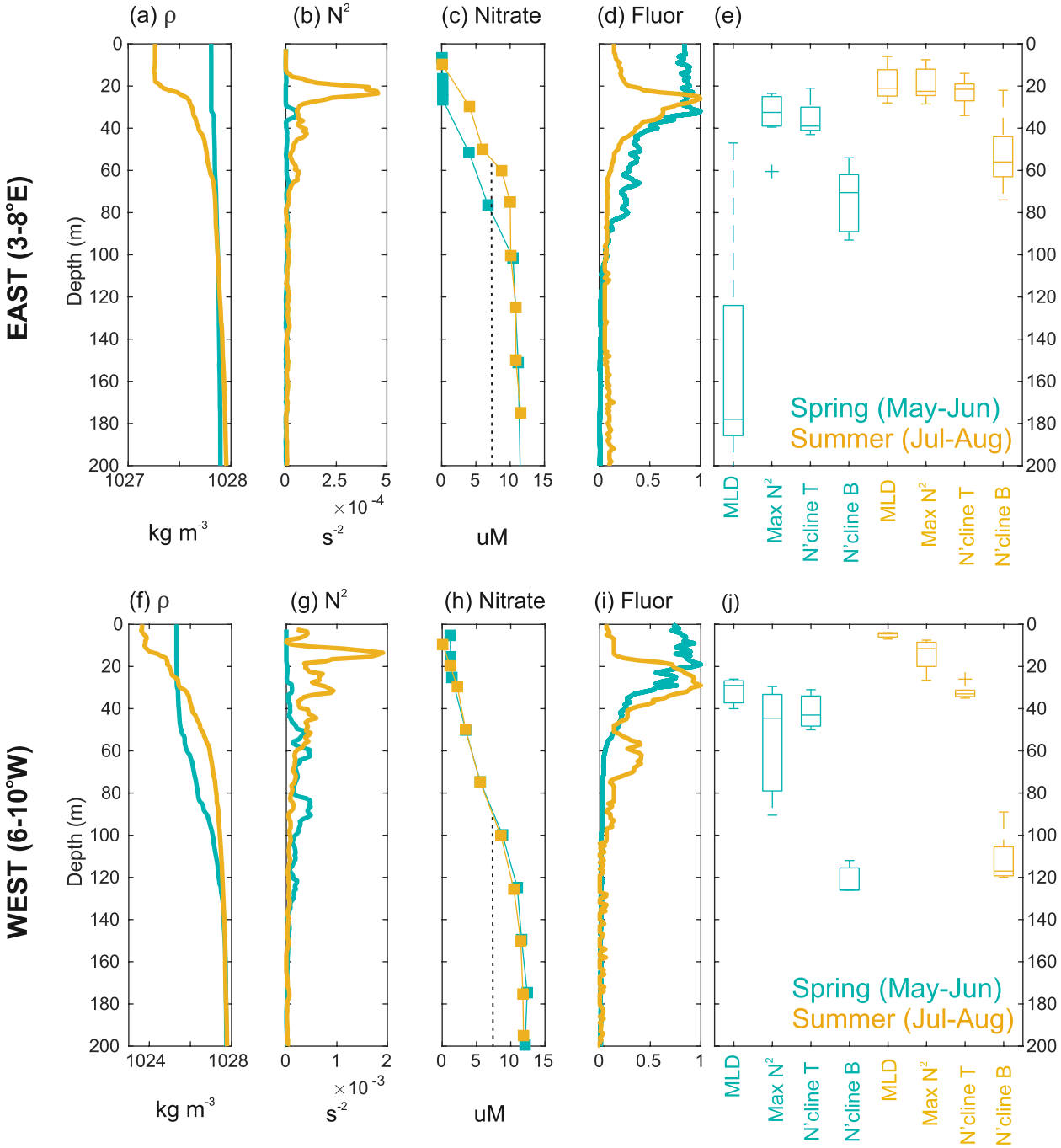

Figure 4. Representative profiles of potential density (a, f; kg m^{-3}), buoyancy frequency (b, g; N^2; s^{-2}), nitrate (c, h; μM), and normalized chlorophyll-*a* fluorescence (d, i) on the eastern (top; 3°–8°E) and western (bottom; 6°–10°W) sides of the Fram Strait in May–June (blue) and July–August (red). Note that the scales in potential density and buoyancy frequency are different between the top and bottom panels. Chlorophyll-*a* fluorescence profiles have been normalized based on the maximum and minimum values over the top 200 m so that the vertical structures in each season can be more easily seen. The vertical dashed line in panels (c) and (h) is at 7 μM. (e, j) Box and whisker plots of the mixed layer depth (MLD), the depth of the maximum buoyancy frequency (N^2), the top (N'cline T), and bottom (N'cline B) of the nitracline for all profiles on the east (3°–8°E) and west (6°–10°W) of the Fram Strait in each season. On each box, the central mark indicates the median, and the bottom and top edges of the box indicate the 25th and 75th percentiles, respectively. The whiskers extend to the most extreme data points not considered outliers, and the outliers are plotted individually using the "+" symbol.

3.2. Nutrient Concentrations and Isotopic Ratios

Surface water nitrate was low from nitrate uptake by phytoplankton (Figures 2 and 3c). To the east of the Fram Strait, nitrate below the mixed layer in Atlantic origin water was 11.6 ± 0.8 μM (Figures 2 and 3c and Table 1). In the western Fram Strait, nitrate in PSW found beneath the mixed layer was lower, 7.2 ± 2.3 μM, demonstrating a transfer of low nitrate waters from within the central Arctic basin (Randelhoff et al., 2020). Nitrate within the deeper Atlantic origin water on the western side of the Fram Strait was higher (~11 μM). Silicate concentrations were depleted to below 4 μM through the upper 200 m of the AW, a contrast to the PSW where concentrations often exceeded 6 μM in the upper 100 m. During summer, nitrate in the mixed layer was increasingly depleted in both water masses, in the AW nitrate decreased from 5.1 ± 4.0 to 0.9 ± 1.3 μM and in the PSW nitrate decreased from 1.6 ± 1.3 to 0.5 ± 0.4 μM.

The eastern Fram Strait had high N* (−1.4 ± 1.4 μM), close to average phytoplankton requirements, and a low Si*, indicating a silicate deficit (−7.1 ± 0.7 μM) (Figure 5a and Table 1). In the west, the PSW was more N depleted (N* = −4.4 ± 2.4 μM) and relatively Si rich (Si* = −1.4 ± 2.7 μM). In both water masses, by summer, mixed layer Si* had increased (in the AW from −2.7 ± 3.3 μM in spring to −0.1 ± 0.7 μM in summer and in the PSW from 1.7 ± 2.6 to 4.5 ± 2.1 μM) as nitrate became more depleted relative to silicate.

In the east, the nitrate transported in AW (below 100 m depth) had a δ^{15}N-NO_3 value of 5.1‰ ± 0.2‰, which is comparable to values entering the Barents Sea and those from the North Atlantic Ocean (Peng et al., 2018; Van Oostende et al., 2017). This suggests that δ^{15}N-NO_3 has not been modified in transit from the subpolar North Atlantic through uptake and regeneration processes. δ^{18}O-NO_3 was elevated to 2.4‰ ± 0.4‰ in AW. This is comparable to preformed values across the Barents Sea Opening (Tuerena et al., 2021) and results from partial nitrate assimilation followed by nitrification and mixing occurring in transit from the subpolar North Atlantic, causing δ^{18}O-NO_3 to drift upward as the δ^{18}O-NO_3 consumed is lower than the δ^{18}O-NO_3 produced (Peng et al., 2018).

In the west, PSW exiting the Arctic via the Fram Strait contains waters which have been transported through the Barents, Kara, and Laptev Seas, where they are susceptible to modification processes such as nitrate regeneration and denitrification occurring on these shelves (Wefing et al., 2019). The outflowing PSW therefore has an imprint of the eastern and western Arctic shelf signals and that of the Transpolar Drift; their proportions dependent on the strength of the Beaufort Gyre, the pathway of the Transpolar Drift, and the location of the Pacific–Arctic front located near the Lomonosov Ridge (Proshutinsky & Johnson, 1997; Steele et al., 2004). The PSW has relatively high concentrations of phosphate and silicate but relatively low concentrations of nitrate (Torres-Valdes et al., 2013). Below 75 m depth (below the surface mixed layer), we measured δ^{15}N-NO_3 and δ^{18}O-NO_3 of 5.6‰ ± 0.4‰ and 1.5‰ ± 0.5‰, respectively (Table 1), which are similar to values measured by Fripiat et al. (2018) in the northern Fram Strait (~82.5°N). High δ^{15}N-NO_3 and low δ^{18}O-NO_3 represent an Arctic signal from Pacific origin waters alongside the influence of benthic denitrification and nitrate regeneration from the Arctic basin (Granger et al., 2018). The lower δ^{15}N-NO_3 and higher δ^{18}O-NO_3 compared to the Pacific source and East Siberian Sea (Figure 5b) represent a more widespread nitrate source from both Pacific and Atlantic influenced shelves (Fripiat et al., 2018).

Nitrate isotope values were enriched in all surface waters across the Fram Strait, revealing the importance of nitrate uptake by phytoplankton elevating δ^{15}N-NO_3 and δ^{18}O-NO_3 above deep water values (Sigman et al., 1999) (Figures 2, 3g and 3h). During summer, nitrate concentrations in surface waters were often below our measurement limit for nitrate isotopes, preventing the expected higher values being measured. In general, the more elevated nitrate isotope signatures were associated with higher δ^{15}N-PN, as the heavier isotope signature was progressively taken up by phytoplankton as the season progressed (Figure 5).

By considering the tracer Δ(15–18), the effects of assimilation are removed allowing the source signals to be viewed more clearly (Figure 5b and Table 1). The Δ(15–18) tracer shows a gradient from lower Δ(15–18) in the east to higher Δ(15–18) in the west (AW 2.7‰ ± 0.5‰ and PSW 4.2‰ ± 0.7‰). The low Δ(15–18) in AW has been measured in the subpolar North Atlantic and Barents Sea (Peng et al., 2018; Tuerena et al., 2021). We identified a significant negative correlation ($r^2 = 0.515$, df = 21, $p \leq 0.0002$) between Δ(15–18) and N* (Figure 5b). The linear relationship suggests that the signal of low N* and high Δ(15–18) in the PSW is a far-field signal which has been exported from the Arctic basin and carried south within the EGC. The Δ(15–18) measured in the PSW is lower than measurements from the East Siberian Sea (Figure 5, Fripiat et al., 2018),

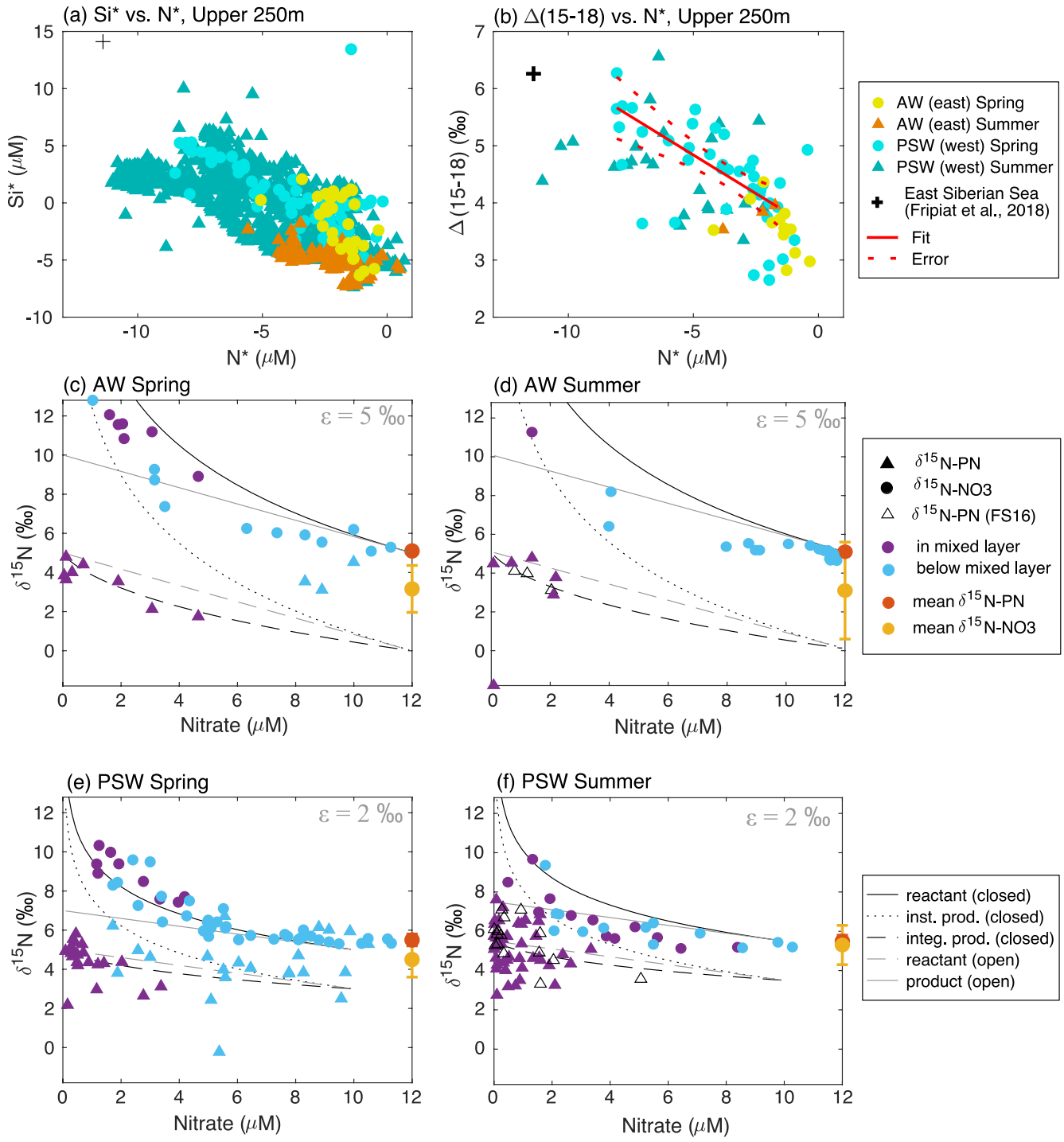

Figure 5. (a) N* plotted against Si* (μM) and (b) N* plotted against Δ(15–18) (‰). (c–f) Uptake fractionation of δ^{15}N-NO_3 (circles) and δ^{15}N-PN (triangles) from JR17005 and PS100. (c) Samples from Atlantic Water during May–June 2018 (JR17005). (d) Samples from Atlantic Water during July–August 2016 (PS100). (e) Samples from Polar Surface Water during May–June 2018 (JR17005). (f) Samples from Polar Surface Water during July–August 2016 (PS100). Additional black open triangles in panels (d) and (f) are δ^{15}N-PN values in the mixed layer in August–September 2016 from cruise FS16. Black and gray lines describe the fractionation trends for an isotopic effect of 5‰ (AW) and 2‰ (PSW).

likely from mixing with Eurasian influenced shelves suggesting a diluted Pacific source signal exiting the Fram Strait.

4. Discussion

4.1. Present Day Fram Strait Dynamics

We have identified strong west-east differences in our data originating from the far-field transfer of hydrographic and biogeochemical properties, from the North Atlantic (eastern Fram Strait) and central Arctic basin (western Fram Strait). Our isotopic data can be further used to determine the effects of these properties on N uptake and limitation.

In AW, weak stratification, a deep mixed layer, and a shallow nitracline during spring (Figure 4e) are likely to have facilitated wind-driven vertical mixing of nitrate into the euphotic zone and the even distribution of chlorophyll-*a* between the surface and top of the nitracline (Figures 4c–4e). The AW was most represented by an open system for samples in the upper 200 m, suggesting ample replenishment of nitrate used by phytoplankton (Figure 5c). In spring, δ^{15}N-PN was 3‰ ± 1.2‰, the low δ^{15}N-PN (lower than the nitrate source of ∼5‰) reflects incomplete nitrate utilization and resupply of nutrients within the deep mixed layer. In summer, increased stratification and shoaling of the MLD to ∼20 m restricted the vertical supply of nutrients. However, average δ^{15}N-PN remained low in summer (3.1‰ ± 2.5‰ during July–August and 3.6‰ ± 0.5‰ in August–September, Figure 5d and Table 1), suggesting that even in late summer, NPP was not strongly limited by N. This finding corroborates recent work that AWs in the Fram Strait are colimited by Fe and Si (Krisch et al., 2020). Overall, in the eastern Fram Strait, there are more nutrients available to phytoplankton, likely supporting higher NPP compared to the western Fram Strait.

In contrast, strong salinity stratification in PSW prevented MLDs from reaching the nitracline in both spring and summer (Figure 4j). Decoupling of surface waters from the nitracline reduced the potential vertical supply of new nitrate to phytoplankton (Figure 4). This was reflected in our isotopic measurements, which showed closed system dynamics and a low isotope effect of ∼2‰ (Figures 5d and 5e). The lower isotope effect is a common feature of N-limited algae (Needoba & Harrison, 2004) and is present in the mixed layer of salinity stratified Arctic waters (Tuerena et al., 2021). δ^{15}N-PN was high throughout spring and summer and matched the nutrient source by late summer (Table 1), highlighting the stratified environment with stronger N limitation to local phytoplankton.

4.2. Simulated Changes in Atlantic and Polar Surface Water

Using a biogeochemical model hindcast simulation from 1970 to 2019 (see Section 2), we assessed how intra- and inter-annual changes in stratification and winter MLDs (taken as a proxy for the depth of maximum winter mixing) controlled nitrate cycling and its isotopes in PSW and AW. It should be noted that the coarseness of our model substantially degraded the local circulation, causing a weak WSC that was overcome by PSW in the eastern Fram Strait. The importance of eddy-driven transport across the Fram Strait is clear (Fieg et al., 2010; Hattermann et al., 2016; Wekerle et al., 2017), but coarse resolution was a consequence of resolving the complex cycling of nitrogen and its isotopes, requiring dozens of tracers. To alleviate the physical biases, we widened our region of focus to include the Greenland Sea where PSW and AW dominated the west and east, respectively.

The hydrography of PSW and AW over the Greenland Sea was well reproduced by the simulation and showed strong qualitative agreement with field data taken in 2016 and 2018 (Figures S3 and S4), as well as strong multiannual trends in the region that replicated observations. Surface water over the Greenland Shelf, west Greenland Sea, and Iceland Sea freshened at rates of roughly −0.05 psu per decade (Figure 6a), consistent with observed changes in salinity of the EGC since the mid-1980s (Larsen et al., 2016). On the eastern side of the Greenland Sea and in the Loften and Norwegian Basins, there was an increase in salinity that exceeded 0.02 psu per decade (Figure 7a), also consistent with observational evidence since the 1990s (Beszczynska-Möller et al., 2012; Larsen et al., 2016; Lauvset et al., 2018). The salinity trends were strongest over the upper 200 m and were accompanied by warming trends across the region (Figure 6b). Warming was, however, strongest in the east, with trends in temperature as high as 0.5°C per decade, similar

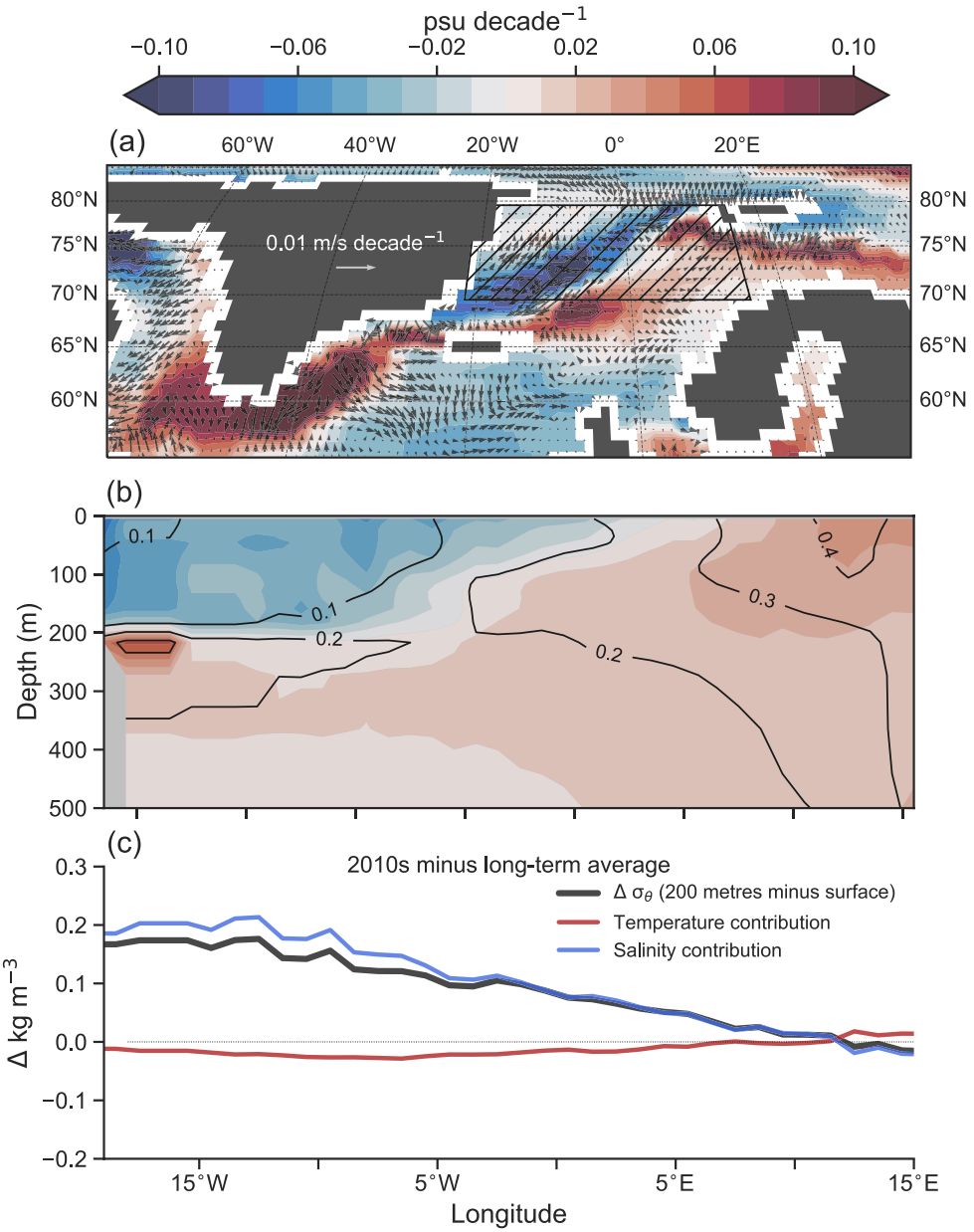

Figure 6. Simulated hydrographic trends in Polar Surface Water and Atlantic Water from 1970 to 2019. (a) Linear, interannual trends in mixed layer salinity (shading) and transport (vectors). (b) Linear, interannual trends in salinity (shading) and potential temperature (black contours) averaged over latitudes 70°–80°N. (c) Difference in upper 200 m density gradient in the final decade (2010–2019) of the simulation compared with the 1970–2019 average, and the changes in the thermal and haline contribution.

to observations (Beszczynska-Möller et al., 2012; Lauvset et al., 2018; Skagseth & Mork, 2012; Tsubouchi et al., 2021; Walczowski et al., 2017). Amplified warming in the east relative to the west at similar latitudes strongly suggested that lateral heat transport made an important contribution to local warming. The strongest west-east gradients in temperature and salinity were established between 2010 and 2019 in our model. Freshening strengthened stratification of PSW in the west, whereas in the east the compensating effects of warming and increasing salinity caused small changes to already weak vertical density gradients in AW (Figures 6c and S3).

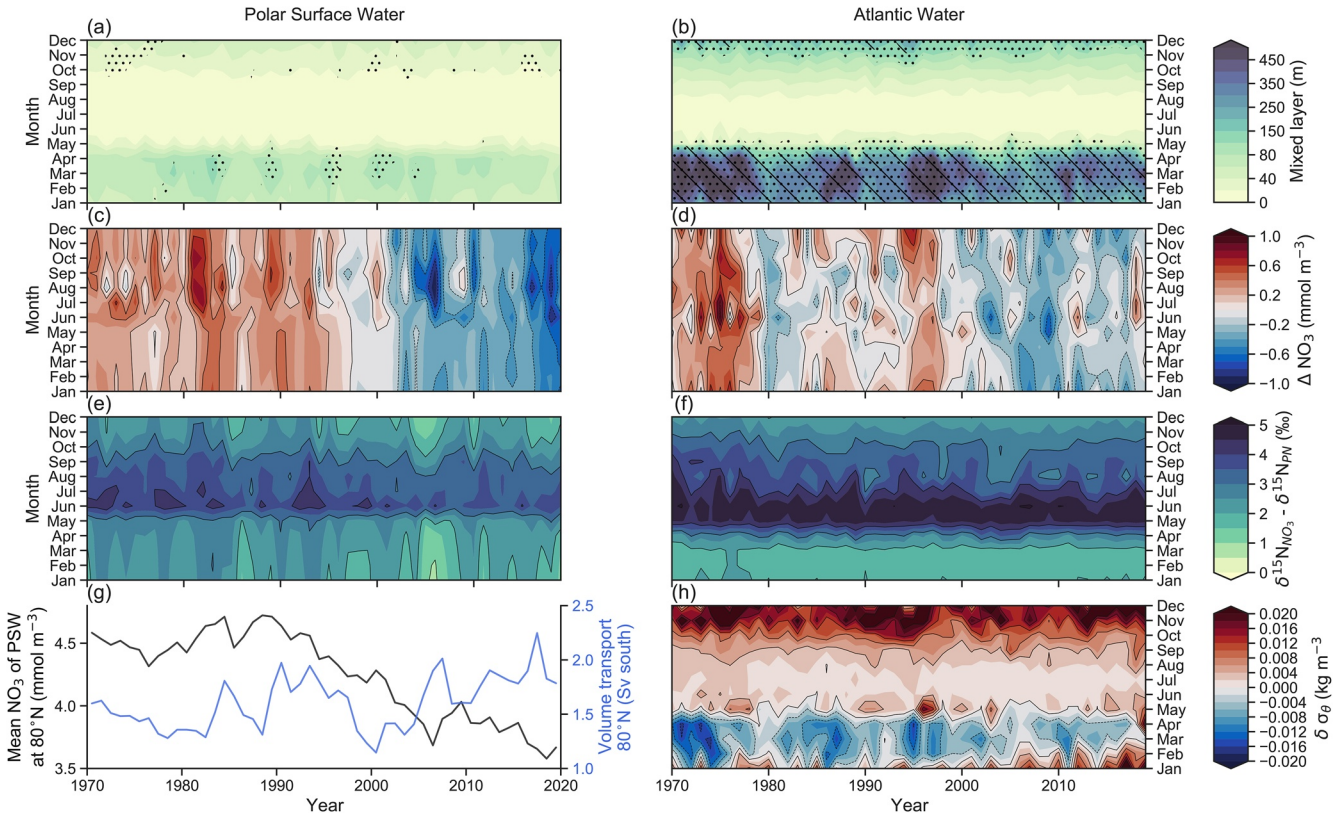

Figure 7. Simulated trends in mixed layer depths, surface nitrate (0–50 m) and their physical drivers from 1970 to 2019 in Polar Surface Water (a, c, d) and Atlantic Water (b, d, f). (a) Average mixed layer depths of PSW. (b) Same as in (a) but for AW. Dots indicate when mixed layers intersect the top of the nitracline, and hatching indicates when mixed layers intersect the bottom of the nitracline. (c, d) Nitrate concentrations in the upper 50 m minus the 1970–2019 average. (e, f) Difference between δ^{15}N-NO_3 and δ^{15}N-PN in upper 50 m. (g) Time series of the mean NO_3 concentration in Polar Surface Water at 80°N across the Fram Strait (black) and the (southward) volume transport (blue) of Polar Surface Water at 80°N. (h) Contribution of salinity to density gradient in the mixed layer averaged over Atlantic Water.

The contrasting PSW and AW hydrography impacted nitrate supply to surface waters. Intense stratification in PSW inhibited vertical supply (Figure 7a). Meanwhile, lateral supply decreased at the beginning of the 1990s and culminated in a loss of roughly 2 μM of nitrate from PSW by 2019 (Figures 7c and 7g). Nitrate limitation in PSW, as observed in our field data, may therefore be a recent consequence of far-field nitrate loss originating in the Arctic, likely driven by upstream increases in primary production (Lewis et al., 2020) and denitrification (Granger et al., 2018) that strip Arctic surface waters of nitrate. Deep winter mixing in AW in the east provided a strong contrast to stratified PSW in the west. Winter mixing consistently intersected the nitracline and replenished nitrate to support the spring bloom (Figure 7b). Phytoplankton within AW experienced nonlimiting nitrate concentrations as a result, and this was also evident in the greater difference between simulated δ^{15}N-NO_3 and δ^{15}N-PN in the east compared to the west (Figures 7e and 7f). However, despite nonlimiting nitrate concentrations, a clear decline in AW nitrate of ~0.5 μM was apparent since the 2000s and paralleled declines in the depth of winter mixing. The relationship between winter–spring (January–May) MLDs and surface nitrate was strong (Spearman's rank correlation; $r^2 = 0.72$), with deep mixing (>400 m) in the 1970s and early 1990s providing as much as 0.8 μM of nitrate more than during shallower winter mixing (250–300 m) in the 1980s and post-2000.

Changes in the depth of winter mixing in AW in our model were primarily driven by a reduction in the influence of sea ice in the region. As sea-ice concentrations declined in the North Greenland Sea and eastern Fram Strait, salt fluxes associated with freezing (i.e., brine rejection) decreased. The contribution of salinity to winter density gradients changed over time during our model experiment, transitioning from a net contribution to mixing (negative downward gradient) to a net contribution to stratification (positive downward gradient) (Figure 7h). By the final years of the simulation, the winter halocline reversed from a

negative to positive gradient for the first time, indicating that winter brine rejection from sea-ice formation was no longer influential. This link between sea-ice formation and deep winter mixing has been previously demonstrated by observations, with buoyancy losses tending to be greatest at the sea-ice edge where brine rejection combines with strong turbulent heat losses (Vage et al., 2018), and is apparent in other models (Brodeau & Koenigk, 2016).

It must be acknowledged, however, that the transition from sea-ice presence to absence occurred much earlier in reality than in our simulation. Like other coarse resolution models (e.g., Brodeau & Koenigk, 2016), we observed a cold bias and too much sea ice in the west and north of the Greenland Sea due to biases in the mean state circulation. In reality, the eastern Fram Strait has been ice free since the early 1980s (Bonnet et al., 2010), likely making heat fluxes the current dominant control on winter mixing rather than sea-ice-associated buoyancy losses. As rapid warming has weakened turbulent heat loss from surface waters in recent decades (Moore et al., 2015), the eastern Fram Strait may have initially experienced weaker winter mixing in the 1980s associated with the transition to sea-ice-free conditions, followed now by further stratification associated with atmospheric warming. Our results therefore suggest that both mechanisms of increasing stratification (less brine rejection and less sea-air heat loss) limit seasonal nitrate replenishment in the eastern Fram Strait. However, multidecadal decreases in mixing in the region are highly uncertain (Brodeau & Koenigk, 2016). Considering the coarseness of our model prevents an accurate representation of important circulation features (Fieg et al., 2010; Hattermann et al., 2016; Wekerle et al., 2017), and predictions of reduced mixing should be viewed with some skepticism. Whatever the direction of change, our field measurements and modeling show that continued monitoring using nitrogen isotopes will reveal if nitrogen is ample or limiting to primary producers.

4.3. Future Prospects for Fram Strait Nutrient Dynamics

In the near future, N limitation may intensify in the western Fram Strait as warming and sea-ice loss stimulate phytoplankton growth in the central Arctic basin and benthic denitrification on Arctic shelves (Arrigo & van Dijken, 2015; Lewis et al., 2020). In the eastern Fram Strait, nutrient supply to surface waters will likely remain stable if winter mixing continues to intersect the nitracline. Observed deep mixing in spring 2018 was sufficient for seasonal nitrate replenishment, indicating that the east-west gradient in nutrient concentrations may strengthen in coming years. Further declines in nitrate supply to the western Fram Strait will reduce NPP and further alter phytoplankton $\delta^{15}N$ with implications for Arctic food web studies (de la Vega et al., 2021). It is important to note that we draw contrasts between distinct water masses on either side of the Fram Strait and acknowledge that the transition between these water masses is unlikely to be linear. The active eddy field and recirculations across the central Fram Strait introduce a host of nonlinear dynamics that mix AW and PSW in highly variable ways.

Over longer time scales of warming, however, winter mixed layers in the east may continue to shoal to depths above the nitracline (Brodeau & Koenigk, 2016; Moore et al., 2015). At present, AWs contribute the majority of the nitrate that supports current NPP in the Fram Strait, implying that any declines in AW nitrate supply could dramatically change NPP in this region. Nitrate in the east is already a primary limiting nutrient to phytoplankton (alongside iron and silicate) (Krisch et al., 2020). Nitrate decline as a consequence of shoaling mixed layers would therefore decrease NPP in the east and potentially increase community recycling of nutrients.

An important consequence of reduced winter mixing in the eastern Fram Strait would be to reduce summertime silicate at a faster rate than nitrate due to the deeper silicicline, potentially increasing silicate limitation in the eastern Fram Strait (Hatún et al., 2017). Although silicate is not a limiting nutrient to all phytoplankton, these changes would alter local phytoplankton assemblages. Diatom limitation and blooms of non-silicifying species, such as *Emiliana huxleyi*, are already observed in the Barents Sea and Fram Strait (Neukermans et al., 2018; Oziel et al., 2020). Diatoms account for much of polar NPP and carbon drawdown (Krause et al., 2019; Vaquer-Sunyer et al., 2013), and thus decreases in silicate availability will affect the strength of the biological pump in this region and also impact food web structure (Vernet et al., 2017).

Our results show that climate change in the short term is unlikely to greatly affect NPP across the Fram Strait in the coming years, with nitrate limitation already resulting in low NPP in the west and deep winter

mixing replenishing nitrate in the east. The decline in nutrient supply to the western Fram Strait is only a small proportion of the N that currently supports NPP across Fram Strait and so these projected declines will not greatly reduce total NPP. However, looking further into the future, if winter MLDs shoal above the nitracline due to rapid atmospheric warming, the ongoing increase in Arctic NPP from alleviated light limitation and terrestrial inputs (Lewis et al., 2020; Terhaar et al., 2021) may be curtailed.

Conflict of Interest

The authors declare no conflicts of interest relevant to this study.

Data Availability Statement

JR17005 data used in this study are available from the following sources: nutrient measurements (Brand et al., 2020, https://doi.org/10.5285/b61d58df-b8e8-11c4-e053-6c86abc0246c), nitrate isotope measurements (Tuerena & Ganeshram, 2021a, https://doi.org/10.5285/b93fb7c0-110e-2470-e053-6c86abc05d60), and δ^{15}N-PN measurements (Norman et al., 2020, https://doi.org/10.5285/b475e367-30e4-5ecf-e053-6c86abc06bd0). PS100 data used in this paper are available from the following sources: nutrient measurements (Graeve & Ludwichowski, 2017, https://doi.org/10.1594/PANGAEA.879197), nitrate isotope measurements (Tuerena & Ganeshram, 2021b, https://doi.org/10.5285/b93fb7c0-110f-2470-e053-6c86abc05d60), and δ^{15}N-PN measurements (Graeve et al., 2019, https://doi.org/10.1594/PANGAEA.902610).

Acknowledgments
The authors thank Celeste Kellock for her assistance with sample collection on cruise JR17005, and S. Torres-Valdes and W. Geibert for collection of samples and logistics on cruise PS100. The authors also thank two anonymous reviewers whose detailed comments and suggestions have greatly improved the manuscript. This work resulted from the ARISE project (NE/P006000/1 awarded to J. Hopkins, NE/P006310/1 awarded to R. S. Ganeshram, and NE/P006035/1 awarded to C. Mahaffey and P. J. Buchanan), part of the Changing Arctic Ocean program, jointly funded by the UKRI Natural Environment Research Council (NERC) and the German Federal Ministry of Education and Research (BMBF). Ship time was provided by AWI-PS100_04. JH was also supported by the Peanuts project NE/R012547/2.

References

Ardyna, M., Babin, M., Gosselin, M., Devred, E., Rainville, L., & Tremblay, J. E. (2014). Recent Arctic Ocean sea ice loss triggers novel fall phytoplankton blooms. *Geophysical Research Letters*, *41*, 6207–6212. https://doi.org/10.1002/2014GL061047

Arrigo, K. R., & van Dijken, G. L. (2015). Continued increases in Arctic Ocean primary production. *Progress in Oceanography*, *136*, 60–70. https://doi.org/10.1016/j.pocean.2015.05.002

Aumont, O., Ethe, C., Tagliabue, A., Bopp, L., & Gehlen, M. (2015). PISCES-v2: An ocean biogeochemical model for carbon and ecosystem studies. *Geoscientific Model Development*, *8*(8), 2465–2513. https://doi.org/10.5194/gmd-8-2465-2015

Beszczynska-Möller, A., Fahrbach, E., Schauer, U., & Hansen, E. (2012). Variability in Atlantic water temperature and transport at the entrance to the Arctic Ocean, 1997–2010. *ICES Journal of Marine Science*, *69*(5), 852–863. https://doi.org/10.1093/icesjms/fss056

Bonnet, S., de Vernal, A., Hillaire-Marcel, C., Radi, T., & Husum, K. (2010). Variability of sea-surface temperature and sea-ice cover in the Fram Strait over the last two millennia. *Marine Micropaleontology*, *74*(3–4), 59–74. https://doi.org/10.1016/j.marmicro.2009.12.001

Brand, T., Norman, L., Mahaffey, C., Tuerena, R., Crocket, K. C., & Henley, S. F. (2020). *Dissolved nutrient samples collected in the Fram Strait as part of the Changing Arctic Ocean programme during cruise JR17005, May–June 2018*. British Oceanographic Data Centre, National Oceanography Centre, NERC.

Brodeau, L., & Koenigk, T. (2016). Extinction of the northern oceanic deep convection in an ensemble of climate model simulations of the 20th and 21st centuries. *Climate Dynamics*, *46*(9–10), 2863–2882. https://doi.org/10.1007/s00382-015-2736-5

Brown, Z. W., Casciotti, K. L., Pickart, R. S., Swift, J. H., & Arrigo, K. R. (2015). Aspects of the marine nitrogen cycle of the Chukchi Sea shelf and Canada Basin. *Deep-Sea Research Part II: Topical Studies in Oceanography*, *118*, 73–87. https://doi.org/10.1016/j.dsr2.2015.02.009

Buchwald, C., Santoro, A. E., McIlvin, M. R., & Casciotti, K. L. (2012). Oxygen isotopic composition of nitrate and nitrite produced by nitrifying cocultures and natural marine assemblages. *Limnology & Oceanography*, *57*(5), 1361–1375. https://doi.org/10.4319/lo.2012.57.5.1361

Casciotti, K. L., Sigman, D. M., Hastings, M. G., Bohlke, J. K., & Hilkert, A. (2002). Measurement of the oxygen isotopic composition of nitrate in seawater and freshwater using the denitrifier method. *Analytical Chemistry*, *74*(19), 4905–4912. https://doi.org/10.1021/ac020113w

Chang, B. X., & Devol, A. H. (2009). Seasonal and spatial patterns of sedimentary denitrification rates in the Chukchi Sea. *Deep-Sea Research Part II: Topical Studies in Oceanography*, *56*(17), 1339–1350. https://doi.org/10.1016/j.dsr2.2008.10.024

Codispoti, L. A., Kelly, V., Thessen, A., Matrai, P., Suttles, S., Hill, V., et al. (2013). Synthesis of primary production in the Arctic Ocean: III. Nitrate and phosphate based estimates of net community production. *Progress in Oceanography*, *110*, 126–150. https://doi.org/10.1016/j.pocean.2012.11.006

de la Vega, C., Mahaffey, C., Tuerena, R. E., Yurkowski, D. J., Ferguson, S. H., Stenson, G. B., et al. (2021). Arctic seals as tracers of environmental and ecological change. *Limnology and Oceanography Letters*. *6*(1), 24–32. https://doi.org/10.1002/lol2.10176

de Steur, L., Hansen, E., Gerdes, R., Karcher, M., Fahrbach, E., & Holfort, J. (2009). Freshwater fluxes in the East Greenland Current: A decade of observations. *Geophysical Research Letters*, *36*, L23611. https://doi.org/10.1029/2009GL041278

de Steur, L., Hansen, E., Mauritzen, C., Beszczynska-Möller, A., & Fahrbach, E. (2014). Impact of recirculation on the East Greenland Current in Fram Strait: Results from moored current meter measurements between 1997 and 2009. *Deep-Sea Research Part I: Oceanographic Research Papers*, *92*, 26–40. https://doi.org/10.1016/j.dsr.2014.05.018

Devol, A. H., Codispoti, L. A., & Christensen, J. P. (1997). Summer and winter denitrification rates in western Arctic shelf sediments. *Continental Shelf Research*, *17*(9), 1029. https://doi.org/10.1016/s0278-4343(97)00003-4

Dodd, P. A., Rabe, B., Hansen, E., Falck, E., Mackensen, A., Rohling, E., et al. (2012). The freshwater composition of the Fram Strait outflow derived from a decade of tracer measurements. *Journal of Geophysical Research*, *117*, C11005. https://doi.org/10.1029/2012JC008011

Fieg, K., Gerdes, R., Fahrbach, E., Beszczynska-Möller, A., & Schauer, U. (2010). Simulation of oceanic volume transports through Fram Strait 1995–2005. *Ocean Dynamics*, *60*, 491–502. https://doi.org/10.1007/s10236-010-0263-9

Francois, R., Altabet, M. A., Yu, E.-F., Sigman, D. M., Bacon, M. P., Frank, M., et al. (1997). Contribution of Southern Ocean surface-water stratification to low atmospheric CO_2 concentrations during the last glacial period. *Nature*, *389*, 929–935. https://doi.org/10.1038/40073

Fripiat, F., Declercq, M., Sapart, C. J., Anderson, L. G., Bruechert, V., Deman, F., et al. (2018). Influence of the bordering shelves on nutrient distribution in the Arctic halocline inferred from water column nitrate isotopes. *Limnology & Oceanography*, *63*(5), 2154–2170. https://doi.org/10.1002/lno.10930

Furevik, T. (2001). Annual and interannual variability of Atlantic Water temperatures in the Norwegian and Barents Seas: 1980–1996. *Deep-Sea Research Part I: Oceanographic Research Papers*, *48*(2), 383–404. https://doi.org/10.1016/s0967-0637(00)00050-9

Graeve, M., & Ludwichowski, K.-U. (2017). *Inorganic nutrients measured on water bottle samples from CTD/large volume water-sampler-system during POLARSTERN cruise PS100 (ARK-XXX/2)*. https://doi.org/10.1594/PANGAEA.879197

Graeve, M., Ludwichowski, K.-U., Müller, S., Guillou, G., & Lebreton, B. (2019). *Stable isotope compositions ($\delta^{13}C$ and $\delta^{15}N$) of seston measured on water bottle samples from CTD/large volume water-sampler-system during POLARSTERN cruise PS100 (ARK-XXX/2)*. https://doi.org/10.1594/PANGAEA.902610

Granger, J., & Sigman, D. M. (2009). Removal of nitrite with sulfamic acid for nitrate N and O isotope analysis with the denitrifier method. *Rapid Communications in Mass Spectrometry*, *23*(23), 3753–3762. https://doi.org/10.1002/rcm.4307

Granger, J., Sigman, D. M., Gagnon, J., Tremblay, J. E., & Mucci, A. (2018). On the properties of the Arctic halocline and deep water masses of the Canada Basin from nitrate isotope ratios. *Journal of Geophysical Research: Oceans*, *123*, 5443–5458. https://doi.org/10.1029/2018JC014110

Granger, J., Sigman, D. M., Needoba, J. A., & Harrison, P. J. (2004). Coupled nitrogen and oxygen isotope fractionation of nitrate during assimilation by cultures of marine phytoplankton. *Limnology & Oceanography*, *49*(5), 1763–1773. https://doi.org/10.4319/lo.2004.49.5.1763

Gruber, N., & Sarmiento, J. L. (1997). Global patterns of marine nitrogen fixation and denitrification. *Global Biogeochemical Cycles*, *11*(2), 235–266. https://doi.org/10.1029/97GB00077

Haine, T. W. N., Curry, B., Gerdes, R., Hansen, E., Karcher, M., Lee, C., et al. (2015). Arctic freshwater export: Status, mechanisms, and prospects. *Global and Planetary Change*, *125*, 13–35. https://doi.org/10.1016/j.gloplacha.2014.11.013

Hattermann, T., Isachsen, P. E., von Appen, W. J., Albretsen, J., & Sundfjord, A. (2016). Eddy-driven recirculation of Atlantic Water in Fram Strait. *Geophysical Research Letters*, *43*, 3406–3414. https://doi.org/10.1002/2016GL068323

Hatún, H., Azetsu-Scott, K., Somavilla, R., Rey, F., Johnson, C., Mathis, M., et al. (2017). The subpolar gyre regulates silicate concentrations in the North Atlantic. *Scientific Reports*, *7*, 14576. https://doi.org/10.1038/s41598-017-14837-4

Hatún, H., Sando, A. B., Drange, H., Hansen, B., & Valdimarsson, H. (2005). Influence of the Atlantic subpolar gyre on the thermohaline circulation. *Science*, *309*(5742), 1841–1844. https://doi.org/10.1126/science.1114777

Havik, L., Pickart, R. S., Vage, K., Torres, D., Thurnherr, A. M., Beszczynska-Möller, A., et al. (2017). Evolution of the East Greenland Current from Fram Strait to Denmark Strait: Synoptic measurements from summer 2012. *Journal of Geophysical Research: Oceans*, *122*, 1974–1994. https://doi.org/10.1002/2016JC012228

Hop, H., Falk-Petersen, S., Svendsen, H., Kwasniewski, S., Pavlov, V., Pavlova, O., & Soreide, J. E. (2006). Physical and biological characteristics of the pelagic system across Fram Strait to Kongsfjorden. *Progress in Oceanography*, *71*(2–4), 182–231. https://doi.org/10.1016/j.pocean.2006.09.007

Hopkins, J., Brennan, D., Abell, R., Sanders, R. W., & Mountifield, D. (2019). *CTD data from NERC changing Arctic Ocean cruise JR17005 on the RRS James Clark Ross, May–June 2018 (Version 2)*. British Oceanographic Data Centre, National Oceanography Centre, NERC.

Jahn, A., Aksenov, Y., de Cuevas, B. A., de Steur, L., Hakkinen, S., Hansen, E., et al. (2012). Arctic Ocean freshwater: How robust are model simulations? *Journal of Geophysical Research*, *117*, C00D16. https://doi.org/10.1029/2012JC007907

Kanzow, T., von Appen, W.-J., Schaffer, J., Köhn, E., Tsubouchi, T., Wilson, N., & Wisotzki, A. (2017). *Physical oceanography measured on water bottle samples from CTD/large volume watersampler-system during POLARSTERN cruise PS100 (ARK-XXX/2)*. https://doi.org/10.1594/PANGAEA.871028

Karcher, M., Gerdes, R., Kauker, F., Koberle, C., & Yashayaev, I. (2005). Arctic Ocean change heralds North Atlantic freshening. *Geophysical Research Letters*, *32*, L21606. https://doi.org/10.1029/2005GL023861

Kemeny, P. C., Weigand, M. A., Zhang, R., Carter, B. R., Karsh, K. L., Fawcett, S. E., & Sigman, D. M. (2016). Enzyme-level interconversion of nitrate and nitrite in the fall mixed layer of the Antarctic Ocean. *Global Biogeochemical Cycles*, *30*, 1069–1085. https://doi.org/10.1002/2015GB005350

Krause, J. W., Schulz, I. K., Rowe, K. A., Dobbins, W., Winding, M. H. S., Sejr, M. K., et al. (2019). Silicic acid limitation drives bloom termination and potential carbon sequestration in an Arctic bloom. *Scientific Reports*, *9*, 8149. https://doi.org/10.1038/s41598-019-44587-4

Krisch, S., Browning, T. J., Graeve, M., Ludwichowski, K.-U., Lodeiro, P., Hopwood, M. J., et al. (2020). The influence of Arctic Fe and Atlantic fixed N on summertime primary production in Fram Strait, North Greenland Sea. *Scientific Reports*, *10*(1), 15230. https://doi.org/10.1038/s41598-020-72100-9

Larsen, K. M. H., Gonzalez-Pola, C., Fratantoni, P., Beszczynska-Möller, A., & Hughes, S. L. (2016). *ICES report on ocean climate 2015 (ICES Cooperative Research Rep. 331)*. https://doi.org/10.17895/ices.pub.5137

Lauvset, S. K., Brakstad, A., Våge, K., Olsen, A., Jeansson, E., & Mork, K. A. (2018). Continued warming, salinification and oxygenation of the Greenland Sea gyre. *Tellus A: Dynamic Meteorology and Oceanography*, *70*(1), 1–9. https://doi.org/10.1080/16000870.2018.1476434

Lewis, K. M., van Dijken, G. L., & Arrigo, K. R. (2020). Changes in phytoplankton concentration now drive increased Arctic Ocean primary production. *Science*, *369*(6500), 198. https://doi.org/10.1126/science.aay8380

Mariotti, A., Germon, J. C., Hubert, P., Kaiser, P., Letolle, R., Tardieux, A., & Tardieux, P. (1981). Experimental determination of nitrogen kinetic isotope fractionation: Some principles; illustration for the denitrification and nitrification processes. *Plant and Soil*, *62*(3), 413–430. https://doi.org/10.1007/bf02374138

Mayot, N., Matrai, P. A., Arjona, A., Belanger, S., Marchese, C., Jaegler, T., et al. (2020). Springtime export of Arctic sea ice influences phytoplankton production in the Greenland Sea. *Journal of Geophysical Research: Oceans*, *125*, e2019JC015799. https://doi.org/10.1029/2019JC015799

Mills, M. M., Brown, Z. W., Laney, S. R., Ortega-Retuerta, E., Lowry, K. E., van Dijken, G. L., & Arrigo, K. R. (2018). Nitrogen limitation of the summer phytoplankton and heterotrophic prokaryote communities in the Chukchi Sea. *Frontiers in Marine Science*, *5*, 362. https://doi.org/10.3389/fmars.2018.00362

Moore, G. W. K., Vage, K., Pickart, R. S., & Renfrew, I. A. (2015). Decreasing intensity of open-ocean convection in the Greenland and Iceland seas. *Nature Climate Change*, *5*(9), 877–882. https://doi.org/10.1038/nclimate2688

Needoba, J. A., & Harrison, P. J. (2004). Influence of low light and a light: Dark cycle on NO_3^- uptake, intracellular NO_3^-, and nitrogen isotope fractionation by marine phytoplankton. *Journal of Phycology*, *40*(3), 505–516. https://doi.org/10.1111/j.1529-8817.2004.03171.x

Neukermans, G., Oziel, L., & Babin, M. (2018). Increased intrusion of warming Atlantic Water leads to rapid expansion of temperate phytoplankton in the Arctic. *Global Change Biology*, *24*(6), 2545–2553. https://doi.org/10.1111/gcb.14075

Norman, L., de la Vega, C., Ball, J., & Mahaffey, C. (2020). *δ^{15}N-PN, δ^{13}C-POC, particulate organic nitrogen and particulate organic carbon measurements from CTD Niskin-collected water column profiles obtained in the Fram Strait during NERC CAO cruise JR17005, May–June 2018*. British Oceanographic Data Centre, National Oceanography Centre, NERC.

Orr, J. C., Najjar, R. G., Aumont, O., Bopp, L., Bullister, J. L., Danabasoglu, G., et al. (2017). Biogeochemical protocols and diagnostics for the CMIP6 Ocean Model Intercomparison Project (OMIP). *Geoscientific Model Development*, *10*(6), 2169–2199. https://doi.org/10.5194/gmd-10-2169-2017

Oziel, L., Baudena, A., Ardyna, M., Massicotte, P., Randelhoff, A., Sallee, J. B., et al. (2020). Faster Atlantic currents drive poleward expansion of temperate phytoplankton in the Arctic Ocean. *Nature Communications*, *11*(1), 1705. https://doi.org/10.1038/s41467-020-15485-5

Peng, X. F., Fawcett, S. E., van Oostende, N., Wolf, M. J., Marconi, D., Sigman, D. M., & Ward, B. B. (2018). Nitrogen uptake and nitrification in the subarctic North Atlantic Ocean. *Limnology & Oceanography*, *63*(4), 1462–1487. https://doi.org/10.1002/lno.10784

Peralta-Ferriz, C., & Woodgate, R. A. (2015). Seasonal and interannual variability of pan-Arctic surface mixed layer properties from 1979 to 2012 from hydrographic data, and the dominance of stratification for multiyear mixed layer depth shoaling. *Progress in Oceanography*, *134*, 19–53. https://doi.org/10.1016/j.pocean.2014.12.005

Polyakov, I. V., Alkire, M. B., Bluhm, B. A., Brown, K. A., Carmack, E. C., Chierici, M., et al. (2020). Borealization of the Arctic Ocean in response to anomalous advection from sub-Arctic seas. *Frontiers in Marine Science*, *7*, 491. https://doi.org/10.3389/fmars.2020.00491

Polyakov, I. V., Pnyushkov, A. V., Alkire, M. B., Ashik, I. M., Baumann, T. M., Carmack, E. C., et al. (2017). Greater role for Atlantic inflows on sea-ice loss in the Eurasian Basin of the Arctic Ocean. *Science*, *356*(6335), 285. https://doi.org/10.1126/science.aai8204

Proshutinsky, A. Y., & Johnson, M. A. (1997). Two circulation regimes of the wind driven Arctic Ocean. *Journal of Geophysical Research*, *102*(C6), 12493–12514. https://doi.org/10.1029/97JC00738

Rafter, P. A., DiFiore, P. J., & Sigman, D. M. (2013). Coupled nitrate nitrogen and oxygen isotopes and organic matter remineralization in the Southern and Pacific Oceans. *Journal of Geophysical Research: Oceans*, *118*, 4781–4794. https://doi.org/10.1002/jgrc.20316

Randelhoff, A., Fer, I., Sundfjord, A., Tremblay, J.-E., & Reigstad, M. (2016). Vertical fluxes of nitrate in the seasonal nitracline of the Atlantic sector of the Arctic Ocean. *Journal of Geophysical Research: Oceans*, *121*, 5282–5295. https://doi.org/10.1002/2016JC011779

Randelhoff, A., Holding, J., Janout, M., Sejr, M. K., Babin, M., Tremblayu, J. E., & Alkire, M. B. (2020). Pan-Arctic Ocean primary production constrained by turbulent nitrate fluxes. *Frontiers in Marine Science*, *7*, 150. https://doi.org/10.3389/fmars.2020.00150

Randelhoff, A., Reigstad, M., Chierici, M., Sundfjord, A., Ivanov, V., Cape, M., et al. (2018). Seasonality of the physical and biogeochemical hydrography in the inflow to the Arctic Ocean through Fram Strait. *Frontiers in Marine Science*, *5*, 224. https://doi.org/10.3389/fmars.2018.00224

Randelhoff, A., Sundfjord, A., & Reigstad, M. (2015). Seasonal variability and fluxes of nitrate in the surface waters over the Arctic shelf slope. *Geophysical Research Letters*, *42*, 3442–3449. https://doi.org/10.1002/2015GL063655

Richter, M. E., von Appen, W. J., & Wekerle, C. (2018). Does the East Greenland Current exist in the northern Fram Strait? *Ocean Science*, *14*(5), 1147–1165. https://doi.org/10.5194/os-14-1147-2018

Sarmiento, J. L., Gruber, N., Brzezinski, M. A., & Dunne, J. P. (2004). High-latitude controls of thermocline nutrients and low latitude biological productivity. *Nature*, *427*(6969), 56–60. https://doi.org/10.1038/nature02127

Schlitzer, R., Anderson, R. F., Dodas, E. M., Lohan, M., Geibere, W., Tagliabue, A., et al. (2018). The GEOTRACES intermediate data product 2017. *Chemical Geology*, *493*, 210–223. https://doi.org/10.1016/j.chemgeo.2018.05.040

Sigman, D. M., Altabet, M. A., McCorkle, D. C., Francois, R., & Fischer, G. (1999). The delta N-15 of nitrate in the Southern Ocean: Consumption of nitrate in surface waters. *Global Biogeochemical Cycles*, *13*(4), 1149–1166. https://doi.org/10.1029/1999GB900038

Sigman, D. M., Casciotti, K. L., Andreani, M., Barford, C., Galanter, M., & Bohlke, J. K. (2001). A bacterial method for the nitrogen isotopic analysis of nitrate in seawater and freshwater. *Analytical Chemistry*, *73*(17), 4145–4153. https://doi.org/10.1021/ac010088e

Sigman, D. M., DiFiore, P. J., Hain, M. P., Deutsch, C., & Karl, D. M. (2009). Sinking organic matter spreads the nitrogen isotope signal of pelagic denitrification in the North Pacific. *Geophysical Research Letters*, *36*, L08605. https://doi.org/10.1029/2008GL035784

Sigman, D. M., DiFiore, P. J., Hain, M. P., Deutsch, C., Wang, Y., Karl, D. M., et al. (2009). The dual isotopes of deep nitrate as a constraint on the cycle and budget of oceanic fixed nitrogen. *Deep-Sea Research Part I: Oceanographic Research Papers*, *56*(9), 1419–1439. https://doi.org/10.1016/j.dsr.2009.04.007

Skagseth, Ø., & Mork, K. A. (2012). Heat content in the Norwegian Sea, 1995–2010. *ICES Journal of Marine Science*, *69*(5), 826–832. https://doi.org/10.1093/icesjms/fss026

Steele, M., & Boyd, T. (1998). Retreat of the cold halocline layer in the Arctic Ocean. *Journal of Geophysical Research*, *103*(C5), 10419–10435. https://doi.org/10.1029/98JC00580

Steele, M., Morison, J., Ermold, W., Rigor, I., Ortmeyer, M., & Shimada, K. (2004). Circulation of summer Pacific halocline water in the Arctic Ocean. *Journal of Geophysical Research*, *109*, C02027. https://doi.org/10.1029/2003JC002009

Terhaar, J., Lauerwald, R., Regnier, P., Gruber, N., & Bopp, L. (2021). Around one third of current Arctic Ocean primary production sustained by rivers and coastal erosion. *Nature Communications*, *12*(1), 169. https://doi.org/10.1038/s41467-020-20470-z

Torres-Valdes, S., Tsubouchi, T., Bacon, S., Naveira-Garabato, A. C., Sanders, R., McLaughlin, F. A., et al. (2013). Export of nutrients from the Arctic Ocean. *Journal of Geophysical Research: Oceans*, *118*, 1625–1644. https://doi.org/10.1002/jgrc.20063

Tsubouchi, T., Våge, K., Hansen, B., Larsen, K., Osterhus, S., Johnson, C., et al. (2021). Increased ocean heat transport into the Nordic Seas and Arctic Ocean over the period 1993–2016. *Nature Climate Change*, *11*, 21–26. https://doi.org/10.1038/s41558-020-00941-3

Tsujino, H., Urakawa, S., Nakano, H., Small, R. J., Kim, W. M., Yeager, S. G., et al. (2018). JRA-55 based surface dataset for driving ocean–sea-ice models (JRA55-do). *Ocean Modelling*, *130*, 79–139. https://doi.org/10.1016/j.ocemod.2018.07.002

Tuerena, R., & Ganeshram, R. (2021a). *Nitrate isotope measurements from CTD Niskin depth profiles from cruise JR17005 in the Fram Strait during May–June 2018*. British Oceanographic Data Centre, National Oceanography Centre, NERC.

Tuerena, R., & Ganeshram, R. (2021b). *Nitrate isotope measurements from CTD Niskin depth profiles from cruise PS100 in the Fram Strait during July–August 2016*. British Oceanographic Data Centre, National Oceanography Centre, NERC.

Tuerena, R. E., Ganeshram, R. S., Geibert, W., Fallick, A. E., Dougans, J., Tait, A., et al. (2015). Nutrient cycling in the Atlantic basin: The evolution of nitrate isotope signatures in water masses. *Global Biogeochemical Cycles*, *29*, 1830–1844. https://doi.org/10.1002/2015GB005164

Tuerena, R. E., Hopkins, J., Ganeshram, R. S., Norman, L., de la Vega, C., Jeffreys, R., & Mahaffey, C. (2021). Nitrate assimilation and regeneration in the Barents Sea: Insights from nitrate isotopes. *Biogeosciences*, *18*, 637–653. https://doi.org/10.5194/bg-18-637-2021

Vage, K., Papritz, L., Havik, L., Spall, M. A., & Moore, G. W. K. (2018). Ocean convection linked to the recent ice edge retreat along east Greenland. *Nature Communications*, *9*, 8. https://doi.org/10.1038/s41467-018-03468-6

Van Oostende, N., Fawcett, S. E., Marconi, D., Lueders-Dumont, J., Sabadel, A. J. M., Woodward, E. M. S., et al. (2017). Variation of summer phytoplankton community composition and its relationship to nitrate and regenerated nitrogen assimilation across the North Atlantic Ocean. *Deep-Sea Research Part I: Oceanographic Research Papers*, *121*, 79–94. https://doi.org/10.1016/j.dsr.2016.12.012

Vaquer-Sunyer, R., Duarte, C. M., Regaudie-de-Gioux, A., Holding, J., Garcia-Corral, L. S., Reigstad, M., & Wassmann, P. (2013). Seasonal patterns in Arctic planktonic metabolism (Fram Strait—Svalbard region). *Biogeosciences*, *10*(3), 1451–1469. https://doi.org/10.5194/bg-10-1451-2013

Vernet, M., Richardson, T. L., Metfies, K., Nothig, E. M., & Peeken, I. (2017). Models of plankton community changes during a warm water anomaly in Arctic waters show altered trophic pathways with minimal changes in carbon export. *Frontiers in Marine Science*, *4*, 160. https://doi.org/10.3389/fmars.2017.00160

von Appen, W. J., Schauer, U., Hattermann, T., & Beszczynska-Möller, A. (2016). Seasonal cycle of mesoscale instability of the West Spitsbergen Current. *Journal of Physical Oceanography*, *46*(4), 1231–1254. https://doi.org/10.1175/jpo-d-15-0184.1

Walczowski, W., Beszczynska-Möller, A., Wieczorek, P., Merchel, M., & Grynczel, A. (2017). Oceanographic observations in the Nordic Sea and Fram Strait in 2016 under the 10 PAN long-term monitoring program AREX. *Oceanologia*, *59*(2), 187–194. https://doi.org/10.1016/j.oceano.2016.12.003

Waser, N. A. D., Harrison, P. J., Nielsen, B., Calvert, S. E., & Turpin, D. H. (1998). Nitrogen isotope fractionation during the uptake and assimilation of nitrate, nitrite, ammonium, and urea by a marine diatom. *Limnology & Oceanography*, *43*(2), 215–224. https://doi.org/10.4319/lo.1998.43.2.0215

Wassmann, P., Slagstad, D., & Ellingsen, I. (2010). Primary production and climatic variability in the European sector of the Arctic Ocean prior to 2007: Preliminary results. *Polar Biology*, *33*(12), 1641–1650. https://doi.org/10.1007/s00300-010-0839-3

Wefing, A. M., Christl, M., Vockenhuber, C., van der Loeff, M. R., & Casacuberta, N. (2019). Tracing Atlantic Waters using I-129 and U-236 in the Fram Strait in 2016. *Journal of Geophysical Research: Oceans*, *124*, 882–896. https://doi.org/10.1029/2018JC014399

Weigand, M. A., Foriel, J., Barnett, B., Oleynik, S., & Sigman, D. M. (2016). Updates to instrumentation and protocols for isotopic analysis of nitrate by the denitrifier method. *Rapid Communications in Mass Spectrometry*, *30*(12), 1365–1383. https://doi.org/10.1002/rcm.7570

Wekerle, C., Wang, Q., von Appen, W.-J., Danilov, S., Schourup-Kristensen, V., & Jung, T. (2017). Eddy-resolving simulation of the Atlantic Water circulation in the Fram Strait with focus on the seasonal cycle. *Journal of Geophysical Research: Oceans*, *122*, 8385–8405. https://doi.org/10.1002/2017JC012974

Woodgate, R. A. (2018). Increases in the Pacific inflow to the Arctic from 1990 to 2015, and insights into seasonal trends and driving mechanisms from year-round Bering Strait mooring data. *Progress in Oceanography*, *160*, 124–154. https://doi.org/10.1016/j.pocean.2017.12.007